UiT The Arctic University of Norway

Faculty of Science and Technology
Department of Physics and Technology

Evaluation of a Solar Power Plant at Longyearbyen

Thomas Oxlund Enoksen
EOM-3901 Master's Thesis in Energy, Climate and Environment
June 2020

UiT The Arctic University of Norway

"If you do not believe you can do it you have no chance at all."

- Arsène Wenger

Abstract

The world face one of the greatest challenges of all time, changing the economy in a direction where higher resource productivity and lower greenhouse gas emissions are the main focus. The most prominent solution to reduce green house gases is a greater utilisation of renewable energy sources. With a rapid technological advancement, solar energy is now one of the least expensive forms of power in two thirds of the world (Olson, 2019). The main aim of the thesis is to find the solar energy potential at Spitsbergen in Norway, by creating a model of a solar plant at Longyearbyen in PVsyst and simulate it. The model is a replica of the solar plant at Svalbard Airport. If the simulations of the plant are accurate with the power yield of the solar plant, the model in PVsyst is confirmed. The model can be used for finding areas of improvement on the plant, and quantify these areas. Further, to find the best use of solar energy in the Arctic, simulations of an optimal generic 10 kW system for standard and bifacial modules with meteorological data from Longyearbyen are run. A similar model is run with meteorological data in Munich to see how the results compare with locations in another climate. This part of the study also includes data from solar modules at the University of Tromsø for comparison.

The results from simulations of the model show a higher total power production than the power yielded from the Airport in 2019 of 9,6%, with multiple areas for improvements on the plant, e. g—oversized inverters and snow cover. Results from simulations of the generic 10 kW system show that the benefits of bifacial modules are more prominent in an Arctic climate than in Munich.

Acknowledgements

Contents

List of Figures

List of Tables

Nomenclature

λ Wavelength (m).

ϕ Photon flux ($\frac{\text{\# of photons}}{s*m^2}$)

I_D Direct irradiance ($\frac{W}{m^2}$)

I_G Global irradiance ($\frac{W}{m^2}$)

K_t Clearness index

$S_{horizontal}$ Global horizontal irradiance ($\frac{W}{m^2}$)

S_{module} Incident solar irradiation on module ($\frac{W}{m^2}$)

V_{oc} Open circuit voltage (V)

AM   Air mass

c   Speed of light ($\frac{m}{s^2}$).

E   Energy of photon (J).

F   Spectral irradiance ($\frac{W}{m^2*\mu m}$)

GCR   Ground cover ratio

H   Power density ($\frac{W}{m^2}$)

h   Planck's constant ($\frac{m^2 kg}{s}$).

m   Length (m)

P   Power (W)

PR   Performance ratio

T   Temperature (°C)

1 Introduction

1.1 Background

As part of the 2015 Paris climate agreement, 189 countries agreed on a common goal to pursue efforts to limit the increase in global temperature to 1.5°C, and stay well below 2°C (Arneth et al., 2019). Public reports commissioned as part of the 2015 Paris agreement present a stark future unless unprecedented changes in all aspects of society are undertaken rapidly (Merchant, 2018). If the 1.5°C goal is to be met, there needs to be a remarkable increase in the percentage of electricity from renewable energies (Merchant, 2018).

Interest in solar energy in Norway was low for a long time, but in recent times the technology has increased significantly in popularity. In 2017, the capacity of solar energy in Norway increased with 59% from 2016, and the increased capacity has continued from year to year (Multiconsult, 2018). The increased interest in solar energy is mainly because of the low costs per megawatt-hour, but the growing interest in renewable energy and sustainability should not be neglected.

In 2016, Avinor started the first renewable energy project in Spitsbergen, installing solar modules on the south side of Svalbard Airport. The Airport lies a couple of kilometers west from Longyearbyen, the largest town on the island of Spitsbergen. Located at a latitude of 78° north, it has 155 polar nights and 130 days of the midnight sun. It is a common assumption that solar energy is not an efficient way to harness energy in the far north or south. How can solar energy be a good idea if it is entirely dark during winter? It is freezing in the north, how can you produce solar energy if the sun cannot warm the land? Some of the limitations are viable and also true, others are myths, but sometimes it can be smart to look at the opportunities as well. It is indeed dark in winter, but that means it is always light during summer, making up for the lack of sunlight in wintertime. Despite long nights and less solar irradiation, there are positive features for PV technology in the north as well. A cold climate is also a highly reflective climate because of snow and ice. If the surroundings of a solar cell are reflective, more energy can be absorbed by the cell. Also, low temperatures lead to an increase in solar cell efficiency, which will be discussed below (Solanki, 2015).

The Norwegian electricity grid does not deliver electricity to Spitsbergen, and the burning of coal is the primary source of energy production on the island. Before this project started, the only source of power on the island was burning coal. Due to the only source of power being coal, electricity prices at Longyearbyen are high, which enhances the competitiveness for photovoltaic (PV) energy in Spitsbergen.

1.2 Idea and aim of Thesis

The idea of the thesis was conceived when talking to a good friend of my family, Charles Kristiansen about my field of study, renewable energy. He is the Airport manager at Alta Airport and was aware of the solar energy project at Svalbard Airport. The idea to investigate the solar energy plant at Longyearbyen was then discussed with Professor Tobias Boström, who suggested to make a model of the system in PVsyst.

This thesis aims to create a model of the solar energy plant at Svalbard Airport. The model should be able to look for areas of improvement in the system. Further, the model can be used as a basis to evaluate the potential for solar energy at Spitsbergen, and compare results with solar potential at locations with a different type of climate.

1.3 Structure of thesis

Chapter 2 provides the basic principles to understand the methodology in the thesis. An introduction to solar energy and basics for PV technology is provided.

Chapter 3 presents the information and methodology used to reach results. The chapter describes the solar plant at Svalbard airport, how it is integrated in PVsyst and how the generic 10 kW system is built.

Chapter 4 holds results and discussions of solar properties at Longyearbyen and sensitive parameters in the simulation. It presents the results of each simulation with a detailed discussion.

Chapter 5 provides a debate about uncertainties and a final summary of the results.

2 Theoretical background

2.1 Solar energy

Solar energy powers the Earth's ecosystem, and is the reason we have wind, rain, desserts and rainforest on the Earth. In other words, solar energy is the fuel powering highly energetic systems on the planet. Indirectly, most of our energy sources except thermal energy and nuclear power stems from solar energy. As an example, fossil fuels are formed from solar energy which has been stored for millions of years.

Solar energy can be described as a parcel of energy, where each parcel is a photon that behaves as a wave. The photons energy is given as:

$$E = \frac{hc}{\lambda} \tag{1}$$

Where h is Planck's constant, λ is the wavelength, and c is the speed of light, which is constant (Honsberg and Bowden, 2019). The unit of energy is Watt (W). The only variable parameter influencing the energy of the photon is its wavelength, where an increase in wavelength causes a decrease in photon energy.

Now that the energy of one photon is established, one can expand this by finding the power density for one specific wavelength. The calculation of power density (H) for a given wavelength is done by multiplying the energy from a photon with a specific wavelength and the photon flux. The photon flux is defined as the number of photons per second per unit area (Honsberg and Bowden, 2019). The power density is expressed as:

$$H = \phi \times \frac{hc}{\lambda} = \phi \times E \tag{2}$$

Where (ϕ) is the photon flux, giving H the units W/m^2. From this, we can describe the spectral irradiance (F), which is the most common way to characterize a light source (Honsberg and Bowden, 2019). The function describes the power density at specific wavelengths. Finding the spectral irradiance is done by dividing the power density of a specific wavelength with that specific wavelength.

$$F(\lambda) = H(\lambda) \frac{1}{\Delta \lambda} \tag{3}$$
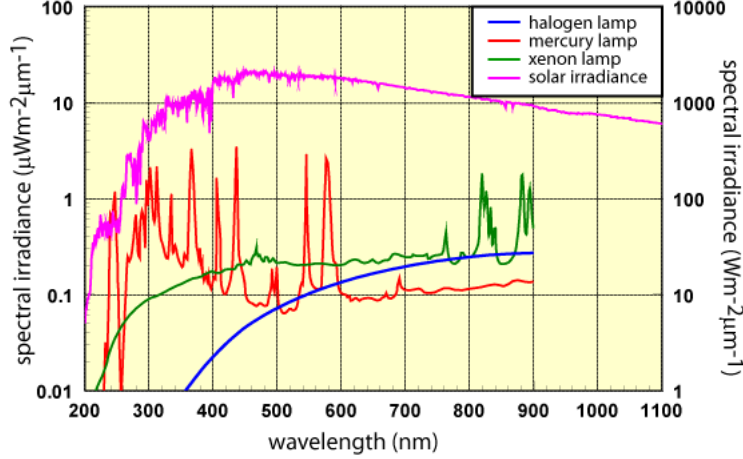
Figure 1: The spectral irradiance of an artificial light-source compared to the spectral irradiance of the sun (Honsberg and Bowden, 2019).

In SI units, the spectral irradiance is $W/m^2\mu m$. Figure 1 shows the spectral irradiance for a variety of light sources. The performance of photovoltaic technology is directly tied to the spectral irradiance emitted from the sun, and the total power density for all wavelengths. Moreover, finding the total power density is essential. Integrating across the spectral irradiance would produce the desired result, but finding a closed-form equation of the spectral irradiance from a light source has proven to be complicated. Instead, the total power density can be found by multiplying the spectral irradiance with the wavelength range over which it was measured which can then be calculated over all wavelengths. (Honsberg and Bowden, 2019). The total power density from the light source is found from the following equation:

$$H = \sum_i F(\lambda_i)\Delta\lambda \qquad (4)$$

Of all light sources, the sun is the most common and exciting source for PV technology. The power density from the sun consists of the whole spectrum of wavelengths, ranging from x-ray radiation to infrared. Assuming the surface temperature of the sun to be 5800 K, the surface luminosity is $64*10^6$ W/m^2 (Honsberg and Bowden, 2019). The total power density at the top of the Earth's atmosphere is approximately 1366 W/m^2 (Nahar, nd).

2.2 Atmospheric effects

Although the suns power density at the top of the atmosphere is somewhere around 1366 W/m², this energy is reduced when reaching the Earth's surface, illustrated in figure 2. When light travels through the atmosphere, photons of each wavelength interact with various parts of the atmosphere due to absorption, scattering and reflection from gases, aerosols and dust. On a clear day, around 77 % of the solar radiation at the top of the atmosphere reaches Earth's surface (Honsberg and Bowden, 2019). The main power reducing factor of solar irradiation is absorption and scattering from air molecules and dust (Honsberg and Bowden, 2019). Most of the infrared light over 2μm is absorbed by either H_2O (water) or CO_2 (carbon dioxide), also known as greenhouse gases. On the opposite side of the sun's irradiance spectrum, most of the absorption of shorter ultraviolet light appears in the ozone layer (Honsberg and Bowden, 2019). As a consequence of absorption and scattering of light, the distance photons travel trough the atmosphere impacts the total power density reaching the Earth's surface.
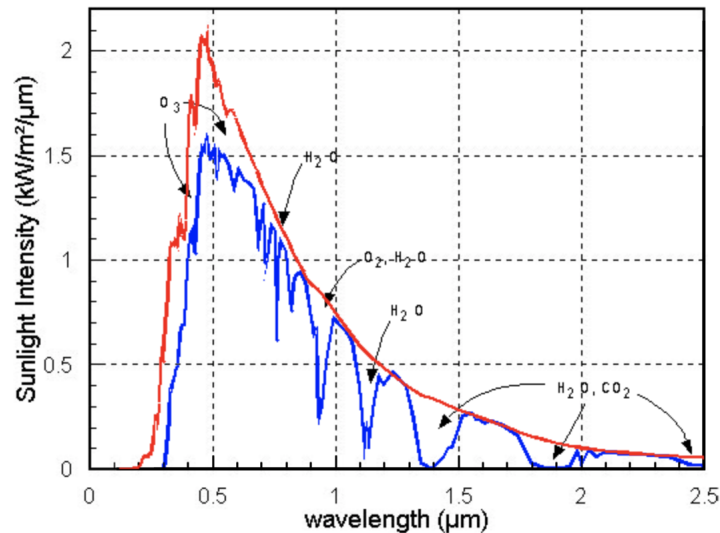
Figure 2: Solar irradiation at top of atmosphere (red), and Earth's surface (Honsberg and Bowden, 2019).

2.2.1 Air Mass

Air mass (AM) is a tool used to calculate the impact of atmospheric effects on power density. It is the pathlength that light travels through the atmosphere normalised to the shortest distance where the sun is directly over one's head (Honsberg and Bowden, 2019). Air mass quantifies the reduction in power when photons travel through the atmosphere (Honsberg and Bowden, 2019), defined in equation 5.

$$AM = \frac{1}{cos(\theta)} \tag{5}$$

Here θ is called the zenith angle, defined as an angle between the sun and the vertical, shown in figure 3. For simplicity, the definition for AM at the top of the atmosphere is air mass 0 (AM0). Intuitively, when the sun is directly over one's head, the air mass is 1 (AM1) because $cos(\theta) = 1$. The problem with equation 5 is that it considers the Earth's surface to be vertically flat. When the sun rises or sets, the zenith angle is 90°, which means the air mass is infinite, although the path length is not. To incorporate the curvature of the Earth equation is expanded (Honsberg and Bowden, 2019).

$$AM = \frac{1}{cos(\theta) + 0.05072(96.0799 - \theta)^{-1.6364}} \tag{6}$$

For locations close to equator equation 5 can be used without any problem. The magnitude of error increases for locations closer to the two poles (Honsberg and Bowden, 2019), so for a location 78° north equation 6 is necessary.
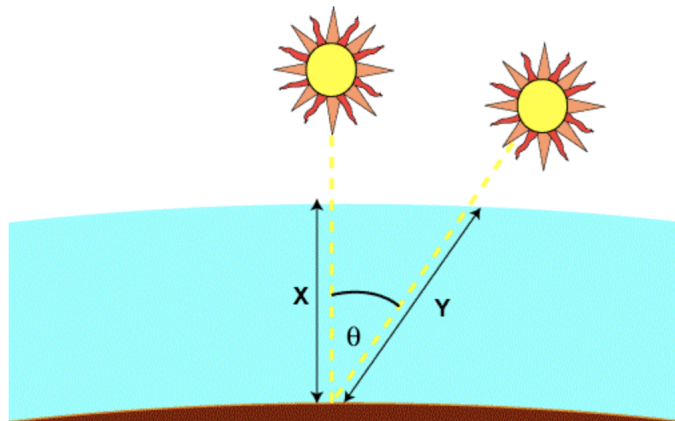
Figure 3: Effect of Air Mass (Honsberg and Bowden, 2019).

2.2.2 Standardisation of Solar Irradiation

The Sun's radiation power and spectrum is not constant, and the variation influences the efficiency of a solar cell (Solanki, 2015). For facilitating accurate comparisons of solar cells measured at different times and locations, a definition of the standard spectrum and power density is made based on air mass (Honsberg and Bowden, 2019). At the Earth's surface, the standard spectrum definition is either AM1.5D or AM1.5G. D stands for direct, meaning direct irradiation only, G stands for global and includes both direct and diffuse irradiation (Honsberg and Bowden, 2019). The irradiation of AM1.5D is a reduction of AM0 with 28%. AM0 is also known as the solar constant. The global spectrum is 10% higher than the direct spectrum, giving AM1.5G a irradiation density of approximately 970 W/m, which is rounded to 1 kW/m^2 since there are variations in the incident solar irradiation (Honsberg and Bowden, 2019). Further, the intensity of the direct component of sunlight (I_D) can be determined as a function of air mass (equation 7). The global component is found by adding 10% (equation 8).

$$I_D = 1.353 * 0.7^{AM^{0.678}} \tag{7}$$

$$I_G = 1.10 * I_D \tag{8}$$

When knowing the zenith angle, equation 8 can then be used to find an estimate of the global irradiation for bright days.

2.3 Declination and Elevation Angle

Now that we know how to calculate the solar irradiation, the declination angle describes how the sun's height above the horizon seasonally varies. The definition of the declination angle is the angle between the equator and a line drawn from the centre of the Earth to the centre of the sun (Honsberg and Bowden, 2019). Since the Earth is tilted by 23.45° on its axis of rotation, the declination angle changes as the Earth orbits the sun. The declination angle is the reason for polar nights and the midnight sun. At the 21st of June, the declination angle is 23.45°, causing the sun to continuously stay above the horizon north of the polar circle. The opposite happens on the 22nd of December. At this date, the declination angle is minus 23.45°, and the sun does not rise above the horizon north of the polar circle. At the spring and fall equinoxes, the declination angle is 0°. The declination angle

impacts the seasonal solar potential at Spitsbergen. Because of its northward location, the solar potential is high in summer, and respectively low in winter.

The elevation angle is the angular height of the sun on the sky measured from the horizontal (Honsberg and Bowden, 2019). The elevation angle varies between 0° and 90° and depends on latitude, declination angle and time throughout the day. During sunrise and sunset, the elevation angle is 0°. When the sun is at a 90° elevation angle, it is located directly over one's head.

2.4   Solar Radiation on a Tilted Surface

At Longyearbyen, the surface irradiation density is low because of its northward location. Tilting a surface perpendicular to the elevation angle maximises the potential irradiation density on the surface. Midsummer in Longyearbyen, the ideal PV modules angle concerning the horizontal is 55°, because of an elevation angle of 35°. The global incident irradiation (GII) on a tilted surface (S_{module}) with an arbitrary angle (β), is found given the global horizontal irradiation (GHI) ($S_{horizontal}$) (Honsberg and Bowden, 2019). The relation between S_{module} and $S_{horizontal}$ is given in equation 9.

$$S_{module} = \frac{S_{horizontal} * sin(\alpha + \beta)}{sin\alpha} \tag{9}$$

Where α is the elevation angle, and β is the angular tilt of the module to the surface (Honsberg and Bowden, 2019).
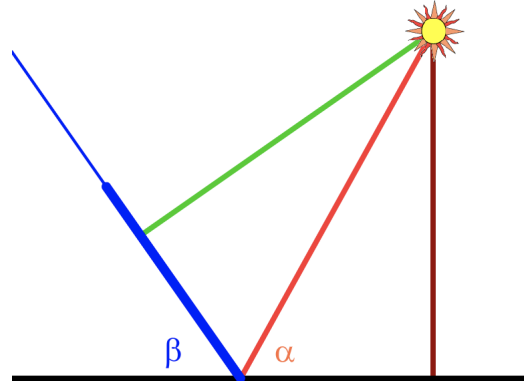
Figure 4: Solar irradiation on a tilted surface. Green line = S_{module}, red line = $S_{incident}$, burgundy line = $S_{horizontal}$ (Honsberg and Bowden, 2019).

2.5 Albedo

Albedo is a measure of reflectance from a body or surface and is the relationship between the reflected electromagnetic radiation, and the incoming irradiation (Store Norske Leksikon, 2018). The albedo is a value between 1 and 0 (National Snow and Ice Datasenter, 2020). If a surface has an albedo value of zero, it is a black body, meaning the object absorbs all irradiation falling on it. On the other hand, if a surface has an albedo value of one, the object reflects all incident irradiation e.g. the snow has a higher albedo than forest or asphalt, because of its greater capacity to reflect light (National Snow and Ice Datasenter, 2020).

2.6 Photovoltaics

Photovoltaic (PV) gets its name from the process of converting light into electricity, which is called the photovoltaic effect (Laboratory, nd). The first type of solar cells came in the 1950s, made from silicon creating an electric current when exposed to sunlight. The first uses of PV technology was for satellites in space and smaller objects such as calculators and watches. In recent years the cost of PV's has declined rapidly, causing it to be the fastest-growing energy resource in the world (Berke, 2018).
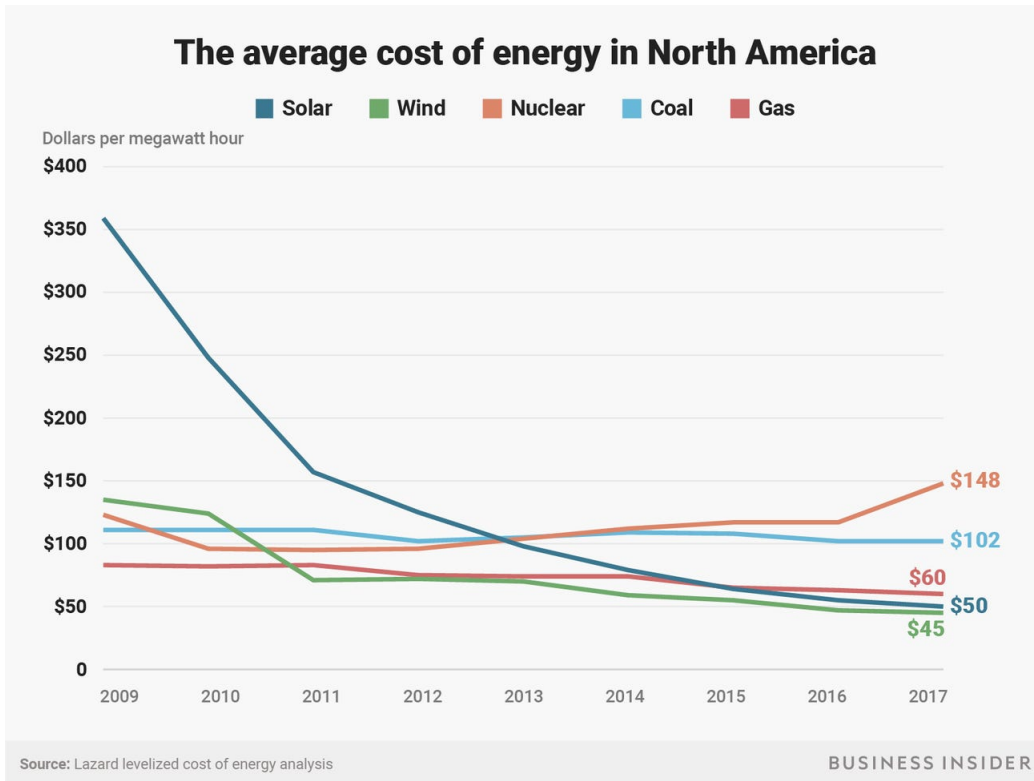
Figure 5: Average cost of energy in North America (Berke, 2018).

2.6.1 Bifacial modules

Bifacial technology is modules which produce electricity on both sides of the panel, with busbars on both sides of its cells (Pickerel, 2018). When installed upon a highly reflecting surface, bi-facial modules are at its most substantial advantage compared to the standard mono-facial module. Solar radiation which initially misses the front side can be reflected to the backside of the module and get absorbed. The higher a bifacial module is elevated, the more power it produces due to its bifacial properties (Pickerel, 2018). Therefore, they perform best on either the ground or flat rooftops because there is room for higher elevation. For locations prone to strong winds, ground-mounted modules are most applicable.

2.6.2 Temperatures Effect on Efficiency

The efficiency of a solar cell is influenced by temperature because the open-circuit voltage (V_{oc}) changes with temperature (Solanki, 2015). V_{oc} is the maximum voltage that can be generated by the solar cell. When temperature increases in the cell, V_{oc} decreases proportionally, thus reducing the efficiency of the cell (Solanki, 2015). For a standard crystalline silicon solar cell, the efficiency increases by 0.4-0.5% per 1° decrease in temperature (Solanki, 2015).

2.6.3 Performance ratio

Performance ratio (PR) is a quality measure of a PV plant. It is the relationship between actual and theoretical energy output for a PV plant (SMA Solar Technology, nd). A value of 100% is not possible because of unavoidable losses in the operation of the PV plant (e. g. thermal- and conduction losses). The theoretical energy output from a PV module is based on performance characteristics determined under standard test conditions (STD) (1000 W/m^2 and 25°C) SMA Solar Technology (nd). Therefore, local factors deviating from STD, such as the temperature of the PV module and GII, impact the PR. At lower temperatures, PV modules efficiency increases from STD values, generating a higher PR value. On the other hand, an average lower value for the GII on the PV modules decreases the PR value. Degradation of solar cells throughout its lifespan will also harm the PR value. Mono- and polycrystalline solar cells efficiency can decrease with 20% over 20 years (SMA Solar Technology, nd). A high-quality PV plant should reach up to 80% in PR. The PR is often used for comparing performance levels between specific plants, or monitor the status of the plant over a prolonged period.

2.7 Inverter

A solar inverter is an essential component of the solar electric power system, as it converts the direct current (DC) output of the PV solar panels into alternating current (AC) 240 V (LG Solar, 2020). The AC electricity can then be, in this case, fed into the airport. Excess energy can be fed into the public grid or home battery storage. Inverters come in different sizes, and as a rule of thumb, the size of the inverter should be similar to the peak power of the solar panel system it is controlling (energySage, 2016). So, for instance,

an array of 20 solar panels of 327 W should have an inverter sized at 6.5 kW because inverters are most efficient at their designed maximum effect. Other than the size of the solar array, geography and site-specific factors are considered when picking inverter size. At locations with high yearly GHI levels, array systems perform on average closer to their peak, and the inverter's size should be close to the peak power of the solar panel system. If the arrays yield more often is at lower power than its peak, installing a slightly undersized inverter might be more suitable(energySage, 2016).

3 Method

3.1 Svalbard Airport power plant

3.1.1 Surroundings

Svalbard Airport is located at the tip of Adventfjorden, a narrow side fjord to the larger Isfjorden, around 4 km west of Longyearbyen. The Airport is shaded from the south by Platåfjellet. Platåfjellet (455 m.a.s.l) in English means Plateau-mountain and stretches about 5.3 km wide, where the height is approximately uniform across the mountain. The mountain casts shade on the Airport the first month after it returns above the horizon, as well as the last month before it goes below. Other than Platåberget, no surrounding structures are generating significant shading. In the east, Sukkertoppen (424 m.a.s.l) is too far east to impact the modules facing south. In the west, Isfjorden lays over 20 km wide with mountains on the opposite side of the fjord not opposing any shade. In PVsyst the horizon is manually written in, shown in figure 9.

3.1.2 Solar power plant

The renewable energy project at Svalbard Airport started in 2016 and has steadily expanded each year, now consisting of 430 PV modules. The project was initiated by Avinor Svalbard Airport, who wanted to decrease the Airports carbon footprint. Avinor, who is responsible for the daily operations of the Airport, is funding the project. Two types of modules are used, Sunpower-E20-327 and JKM265P.

- 2016 installation:

    - 32 Sunpower e20 roof-mounted with an inclination of 15°, 16 modules are facing −70° east-south, 16 modules are facing 110° west-north.

    - 24 Sunpower e20 wall-mounted on terminal, facing 20° south-west.

- Expansion 2017:

    - 80 Sunpower e20 wall-mounted on terminal, facing 20° south-west.

    - 80 Jinko 265 W wall-mounted on hangar, facing 20° south-west.

- Expansion 2018:

    – 70 Jinko 265 W wall-mounted on hangar, facing 20° south-west.

    – 80 Sunpower e20 wall-mounted on hangar, facing 110°west-north.

    – 60 Sunpower e20 wall-mounted on hangar, facing 20° south-west.

    – 24 Sunpower e20 wall-mounted on air tower, facing 20° south-west.

Total power installed is 137 kWp divided over 300 SPR-20-327 modules and 150 JKM265P. To this date 32 modules are roof-mounted and 418 wall-mounted. The total power production from the system in 2019 was 68,31 MWh.

3.1.3   SPR-E20-327

The SPR-E20-327 solar module is produced by Sunpower, an American company founded in 1985 that specialises in innovative solar technology (Sunpower, 2019). The module has a power warranty that guarantees 95% efficiency for the first five years with the degradation of 0,4% per year for the next 20 years. The average power efficiency is 20,4% with an area of 1,552 m^2(Sunpower, 2016). The power temperature coefficient is -0,35%/°C.

3.1.4   JKM265P

JKM265P is produced by Jinko solar, also an American company. The module has high low light performance and good resilience in extreme weather, criteria highly relevant at Longyearbyen (Jinko Solar, 2015). The JKM265 has a significantly lower efficiency compared to SPR-e20, laying at 16,19% (Jinko Solar, 2015). The degradation rate is -2,5% for the first year and further -0,625% per year until it reaches 25 years (Jinko Solar, 2015). The power temperature coefficient for this module is -0.41%/°C (Jinko Solar, 2015).

3.1.5   Inverters

At Svalbard Airport, Fronius inverters sized 20 kW, 15 kW, 12.5 kW and 10 kW are used to control the arrays.

- 4x Fronius 20.0-3, 20 kW:

    – 2 strings, 30 sunpower e20 modules each, 19,62 kWp.

- – 4 strings, 20 Jinko Solar modules each, 21,20 kWp.

- – 2 strings, 24 and 32 sunpower e20 modules, 18,31 kWp.

- 2x Fronius 15-3, 15 kW:

  - – 2 strings, 20 sunpower e20 modules each, 13,08 kWp.

  - – 2 strings, 20 sunpower e20 modules each, 13,08 kWp.

- 2x Fronius 12.5-3, 12,5 kW:

  - – 4 strings, 10 sunpower e20 modules each, 13,08 kWp.

  - – 4 strings, 10 sunpower e20 modules each, 13,08 kWp.

- 4x Fronius 10.0-3, 10 kW:

  - – 2 strings, 12 sunpower e20 modules each, 7,49 kWp.

  - – 2 strings, 13 and 12 Jinko Solar modules, 6,26 kWp.

  - – 2 strings, 13 and 12 Jinko Solar modules, 6,26 kWp.

  - – 2 strings, 10 Jinko Solar modules each, 5,30 kWp.

3.2   PVsyst 7.0

PVsyst 7.0 is a PC software package for study, sizing and data analysis of complete PV systems. It deals with a variety of systems, grid connected, stand-alone, pumping and DC-grid, and includes extensive meteorological and PV system components databases. For the model made in this thesis, a project design is started in PVsyst, which aims to perform a thorough system design using detailed hourly data (PVsyst, 2019b).

3.3   Modelling in PVsyst

3.3.1   Implementing meteorological data

Before defining the system configuration, one needs to define the location of the model and choose meteorological data. Meteorological data for Longyearbyen is found in PVsyst's database. The data is monthly values between 1981-1990 delivered by Meteonorm 7.2. The data characteristics are synthetically generated from monthly values with a stochastic algorithm, into

hourly values. The year 1990 indicates generic data (unspecific year). Data from Meteonorm 7.2 is used in simulation 1. Parameters available from the source file are:

- Horizontal Global Irradiation (GHI)

- Horizontal Diffuse Irradiation

- Ambient Temperature

- Wind Velocity
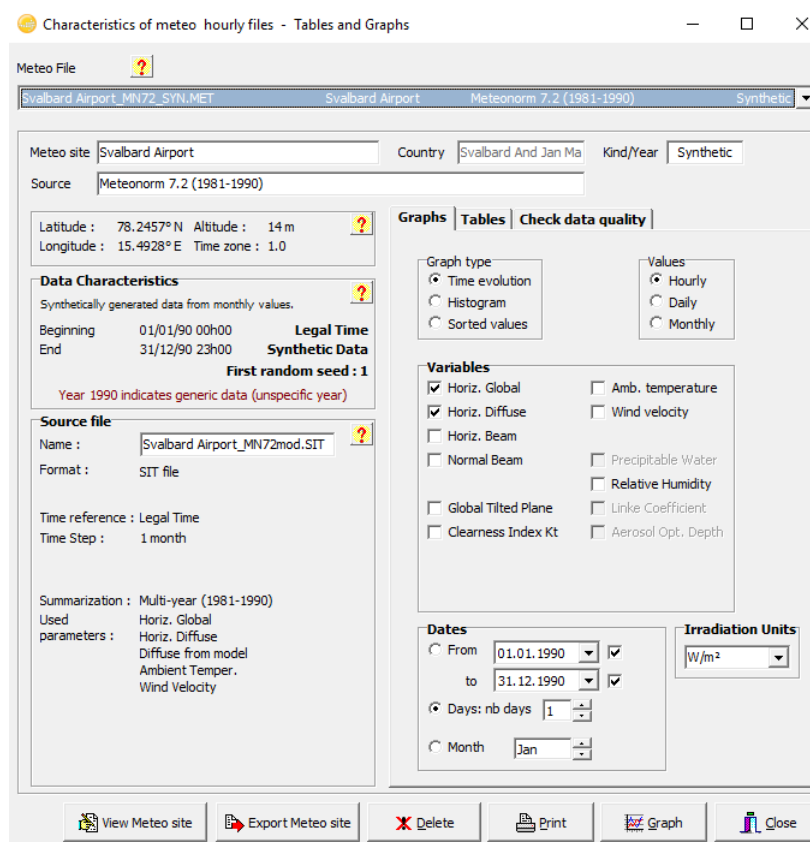
Figure 6: Meteo file used in the first simulation.

One can also incorporate meteorological data manually from an external source. With help from The University Centre in Svalbard (UNIS) recent

meteorological data from Longyearbyen could be used for the system. The weather station is located 10 km outside of Longyearbyen and has been up and running from 2012. The data from UNIS is in 5-minute intervals. The 5-minute intervals are transformed into hourly values before loaded into PVsyst. The source file was created in Excel and saved as a .csv file before loading it into the PVsyst database. Two source files were made. One with data for only 2019, and another with average data from 2015-2017. Ideally, the average data should include more data, but those three years were the only ones with full data sets (measurements taken every 5 minutes for the full year). Meteorological data from the UNIS weather station is implemented into PVsyst from simulation 2 and onwards.

3.3.2 Defining orientation

The next step is to define the orientation of the modules in the model. It is a straightforward process. The field type is set to several orientations, and each orientation and tilt for the system chosen is incorporated.
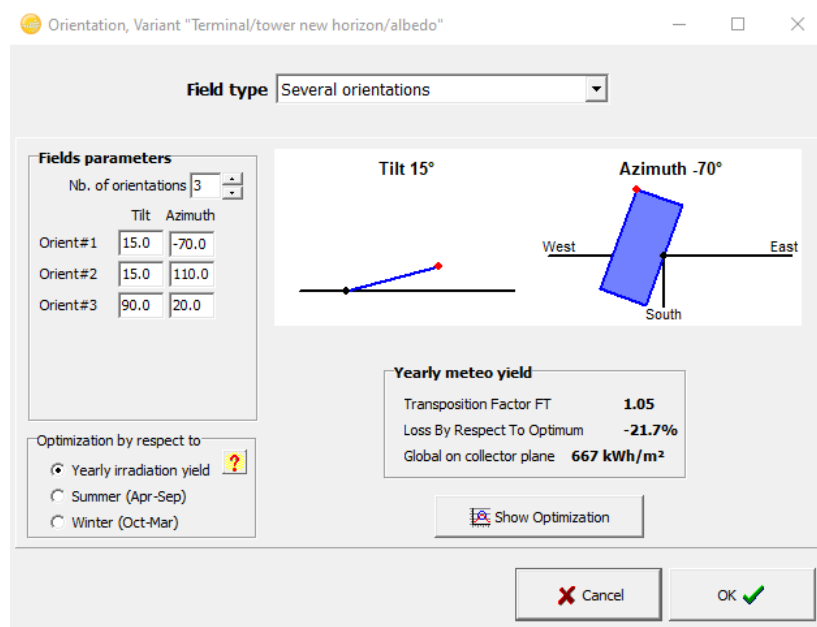
Figure 7: Orientations defined for solar modules on terminal and tower model.

3.3.3 Defining horizon

Using data from Norgeskart, calculations in MatLab provides the solar horizon facing south at Svalbard Airport. The calculations uses the triangles in figure 8 to make a representation of the horizon. The height of the mountain is assumed to be uniform across the edge.
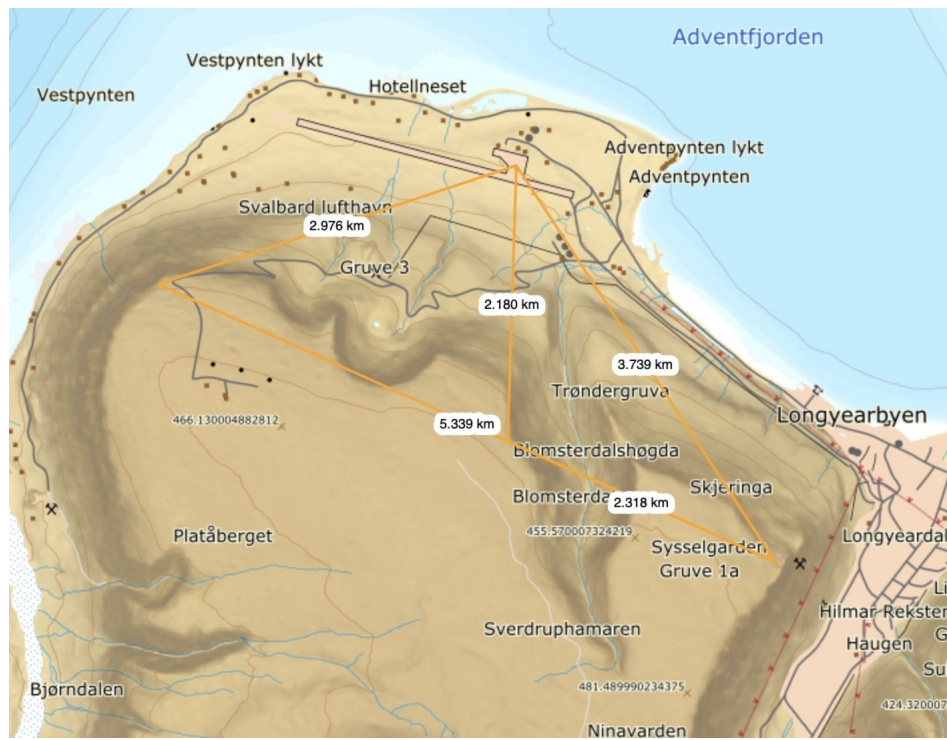
Figure 8: Map of Svalbard Airport and Platåfjellet (Kartverket, 2020).

The horizon is manually implemented based on the MatLab calculations in PVsyst.
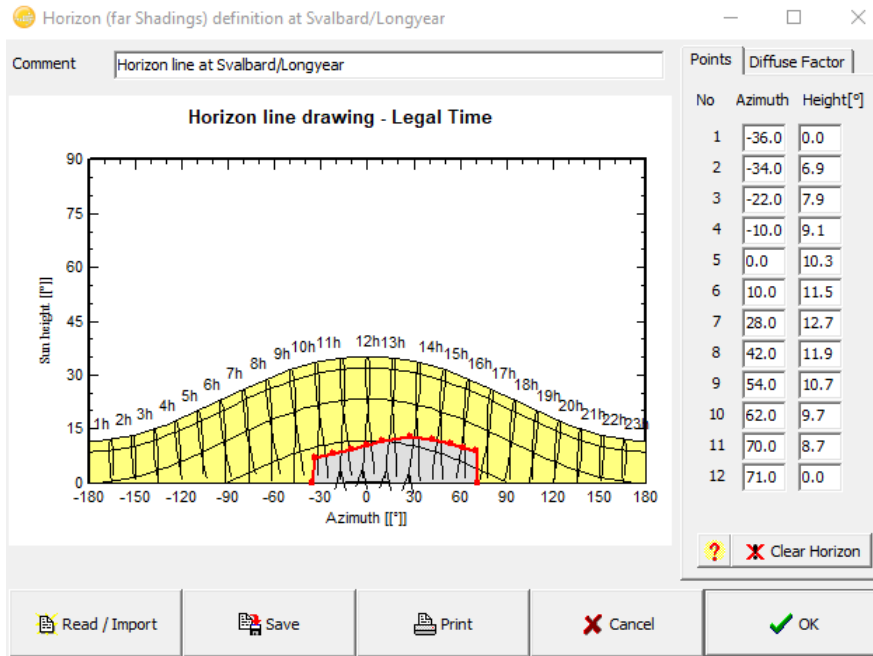
Figure 9: Horizon implemented in PVsyst.

3.3.4 System configuration

The total system configuration is divided by sub-arrays. Solar module type, inverter and solar module configuration are chosen for each sub-array. The most common set up is one inverter for each sub-array. When one inverter controls modules in more than one orientation, two sub-arrays are defined for one inverter. If two configurations are completely alike, one sub-array can be defined for all similar configurations. Implementing this is done by choosing "nb of MPPT inputs" to 2. A overview of two sub-arrays in the system configuration is figure 10 and 11.

The program limits the number of sub-arrays for a simulated system to eight. The most compact way to define the complete Svalbard Airport PV system in PVsyst lead to a use of 10 sub-arrays. Therefore, to model and simulate the entire system at Svalbard Airport, the complete system is divided into two models. The first model is of all solar modules on the terminal building and flight tower. The second model consists of modules on the hangar.

3.3.5 Terminal and tower system

In this system, five sub-arrays are defined, consisting of modules in three orientations. It includes the roof-mounted modules, which have a tilt of 15° and an azimuth angle of -70° and 110°. The 180° between the two sets of roof-mounted modules are because they are faced against each other. The wall-mounted modules in this model have a tilt of 90° and an azimuth angle of 20°. The total size of the system is 220 SPR-e20-327 solar modules, controlled by five inverters, two 20 kW, two 12.5 kW and one 10 kW. Total installed power is 71,9 kWp.
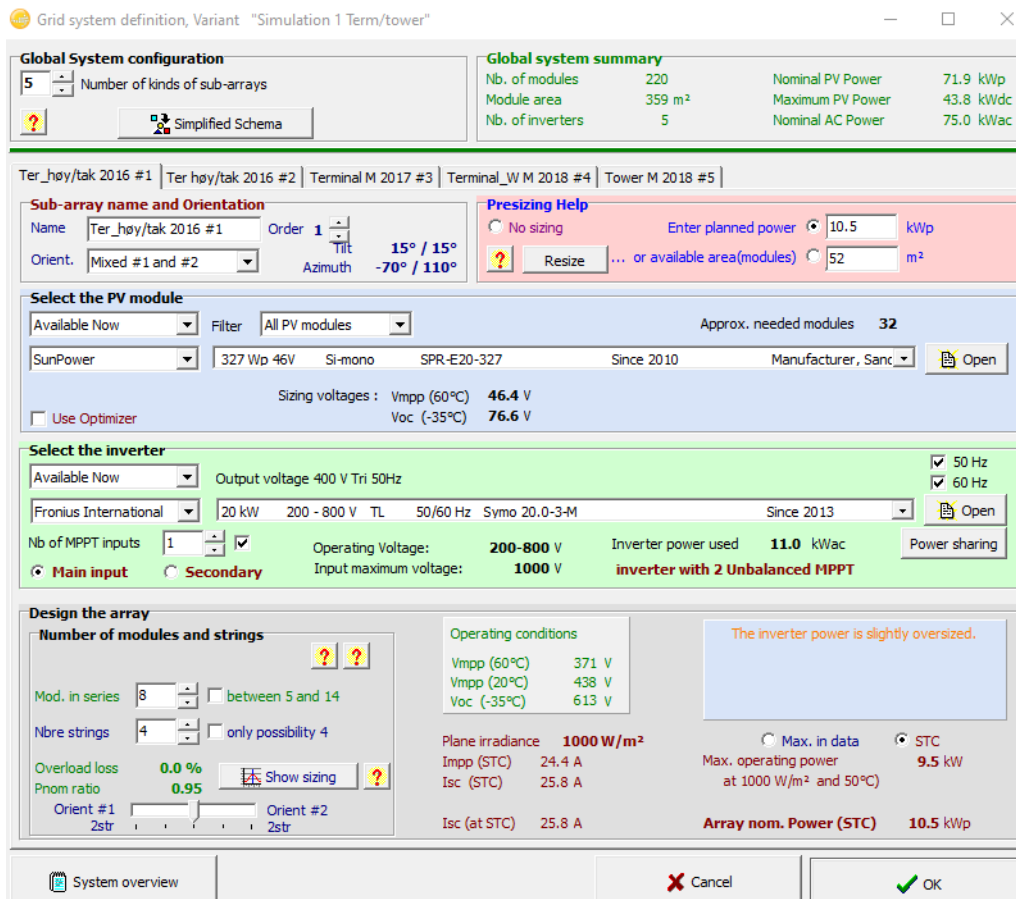
Figure 10: Overview over the sub-arrays made for modules on terminal and tower building.

3.3.6 Hangar system

In this system, five sub-arrays are defined, with modules in two orientations. All modules are wall mounted with a tilt of 90°, with two azimuth angles, respectively 20° and 110°. It consists of 230 modules, 150 JKM 265p and 80 SPR-327, controlled by six inverters, one 20 kW, two 15 kW and three 6 kW. The total installed power is 65,9 kWp.

This system is not wholly similar to the installation at the Airport. The three 10 kW inverters (see section 4.3.5) controlling modules on the hangar are substituted with three 6 kW inverters in the model. Ideally, PVsyst would let the simulation run with 10 kW inverters. However, PVsyst does not allow that, the inverter power is too high with regards to the amount of power the modules can deliver at peak performance.
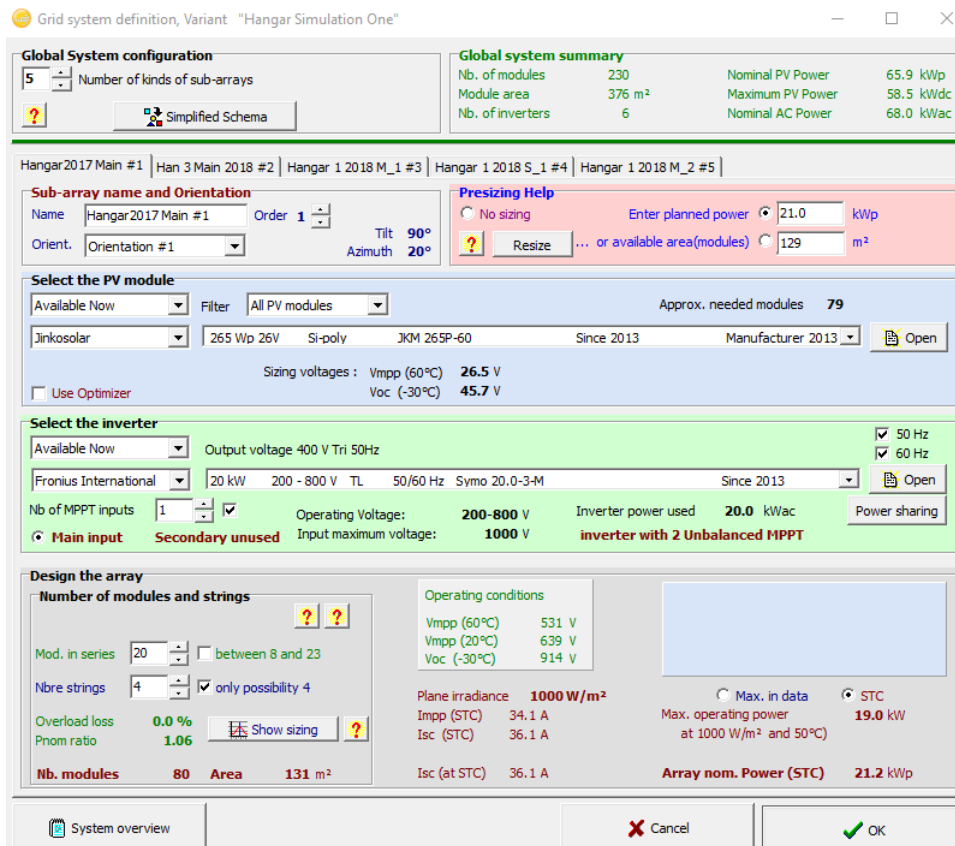
Figure 11: Overview of sub-arrays for modules on hangar building.

3.4 Sensitive parameters in simulation

To methodically make the simulation as similar to the power plant at the Airport as possible, sensitive parameters need to be adjusted to fit with conditions at Longyearbyen. For each simulation of the Svalbard Airport model, changes in one parameter are made before the next simulation takes place.

- First simulation: Run with meteonorm data synthetically generated.

- Second simulation: Change of meteorological data from Meteonorm 7.2 to 2019 data from UNIS i. e. new GHI and temperature.

- Third simulation: Adjusted albedo.

- Fourth simulation: Inverter influence.

- Fifth simulation: Snow cover for roof mounted modules.

3.5   Generic 10kW systems

To find the true potential of standard and bifacial modules at Longyearbyen, a generic 10 kW system is constructed and simulated in PVsyst, and compared with a similar system in Munich, and standard and bifacial modules at the University of Tromsø (UiT). Munich at latitude 48° North is chosen because the location well represents a central Europe climate. Germany also has the highest amount of installed PV power in Europe. To optimise the system as much as possible; the horizon is removed. The reason for setting up the simulation like this is to grant PV production the absolute best conditions as possible within the constraints of PVsyst for bifacial modules.

3.5.1   Standard 10 kW system, Longyearbyen

Ideally, the system's design should be for optimal conditions. For the standard modules, this is not a problem, but simulations cannot be run on a single bifacial module in PVsyst, meaning shade between modules is imposed. To make the comparison between the mono- and the bifacial system as accurate as possible, the same configuration is imposed on both systems. The configuration of modules is explained in the section below. In the configuration, the top of the standard modules are 1,55 meter above the ground when tilted 90°. The system is simulated with a tilt of 90°, 60°, 30° and 0°, with a south/north orientation (SN) (azimuth 0°). The total system consists of 32 modules divided over four strings with a total power of 10,46 kWp, controlled by a 10 kW inverter.

3.5.2   Bifacial 10 kW system, Longyearbyen

When designing a bifacial system, the field type "unlimited sheds" must be chosen. For "unlimited sheds" field-type, the number of sheds (rows of bifacial modules) and length between each shed (pitch) is chosen by the user. From reading the PVsyst's help catalogue and the PVsyst forum, as well as testing the parameters, these values need to be within reasonable numbers for the calculation to give respectable results (PVsyst, 2019a) (PVsyst, 2019c). 11.6° is the shading limit angle picked for the system. This leads

to no shading from one shed on another between the 20th of March to the 23rd of September when modules face SN. The current of the whole string is limited to the current of the weakest cell. The production of the bottom string is null if the lowest cell is fully shaded (PVsyst, 2019b). The number of sheds in the simulation is set to 4 (see figure 13).

Ground cover ratio (GCR): $\frac{A(collector)}{A(ground)}$ is the amount of available ground for the GHI to reflect on the backside of the bifacial modules (PVsyst, 2019b). GCR is the width of the sheds divided by the pitch. If the GCR is low, a lesser fraction of the ground area is shaded.

The 10 kW bifacial system uses LG400N2T-J5 modules, specifications in section 3.5.5. Several simulations with a change in orientation and tilt are made to find to optimal setup for the model. The top of the bifacial modules are 2,04 meters above ground in the model. The paper will evaluate three orientations for bifacial modules, SN, azimuth 45°, and EW (azimuth 90°). For each orientation one simulation is done for each of these tilts: 90°, 60°, 30° and 0°. The system design is 28 bifacial modules 400 W divided over two strings controlled by a 10 kW inverter.
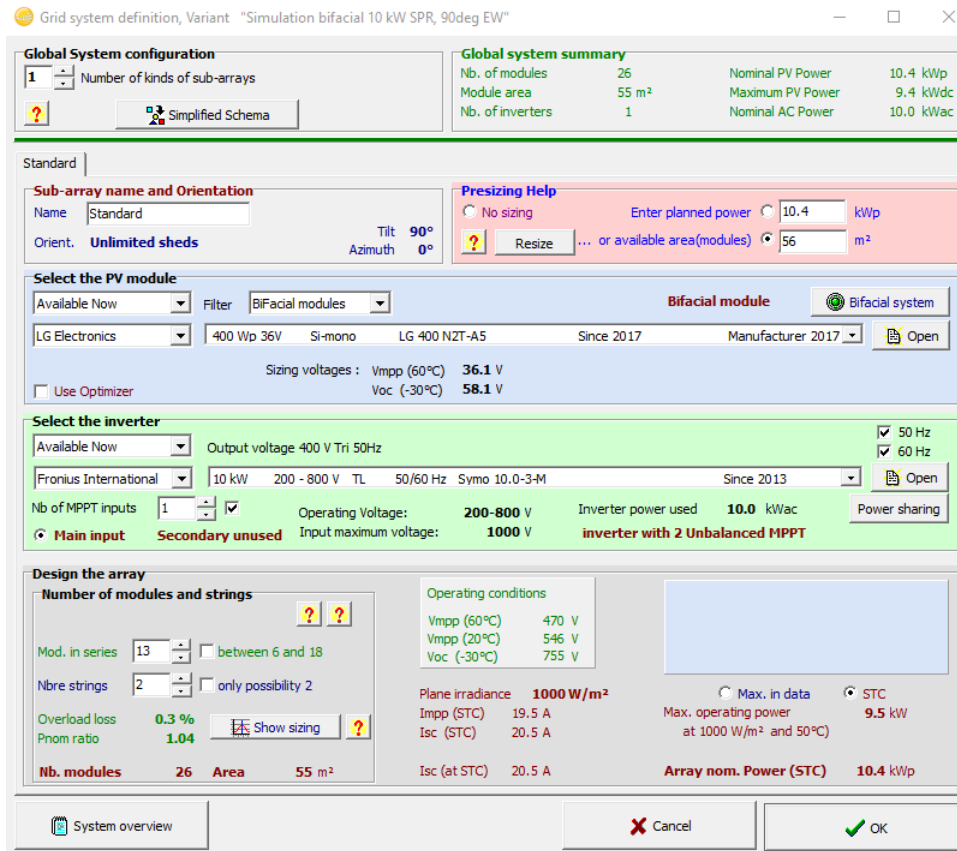
Figure 12: Overview over model made for the generic 10 kW system.
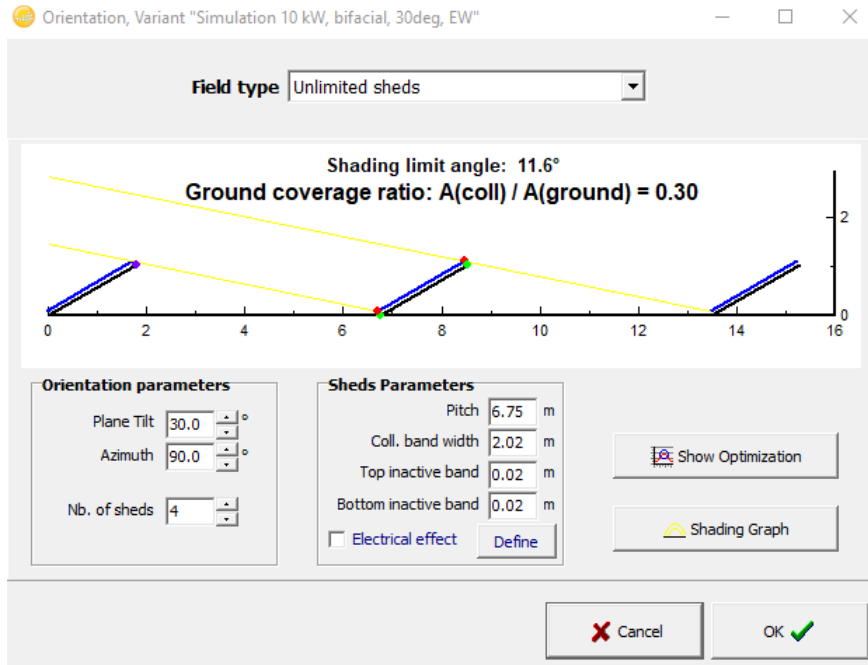
Figure 13: Orientation of bifacial modules to remove shading effects.

3.5.3 Solar modules at UiT

Data from the solar modules at Campus Tromsø was provided by my supervisor, Professor Tobias Boström. The UiT system has both bifacial and standard mono facial modules, and the set-up of modules are seen in figure 14. The modules mounted on the roof face south, while the wall-mounted modules behind face south-west. The UiT modules have practically no shading from nearby objects between azimuth angles of $-90°$ to $90°$. However, the Tromsø system does have some far distance horizon shadowing which has not been quantified.

Figure 14: Solar energy system at UiT, campus Tromsø.

3.5.4   Generic 10 kW system in Munich

A generic 10 kW system is made for mono- and bifacial modules in Munich. For each system, all parameters except albedo and meteorological data is equal to the 10 kW model for Longyearbyen. Simulations are made for SN orientation with tilts 90°, 60° and 30°.

3.5.5   LG400N2T-J5 bifacial solar panel

For the generic simulation of a bifacial system, the 400 W bifacial module from LG electronics is used. The modules length, width and depth is 2,024 m * 1,024 m * 40 mm (electronics, 2019). Its module efficiency is 19,3% and can handle temperatures down to -40°C. Because of its bifacial properties, it is supposed to absorb 30% more light than conventional modules (electronics, 2019).

4 Results and discussion

4.1 Solar-numbers at Longyearbyen

At Longyearbyen, on a midsummers day, the sun is at an elevation angle of 35.2°. This gives a zenith angle (θ) of 54.8°. Using equation 5 from section 2.2.1, the air mass at Longyearbyen when the sun is at its highest is 1,731. Further, the maximum GHI on midsummer's day on a PV module perpendicular to the sun at Longyearbyen is 887 W/m^2, found by putting the air mass at Longyearbyen into equation 7 and 8. Compared to the standard spectrum density at 970 W/m^2, it is approximately 10% lower because of the longer distance light has to travel in the atmosphere to reach Longyearbyen.

4.2 Shading at Svalbard Airport

Plot in MatLab from the calculations of solar horizon.
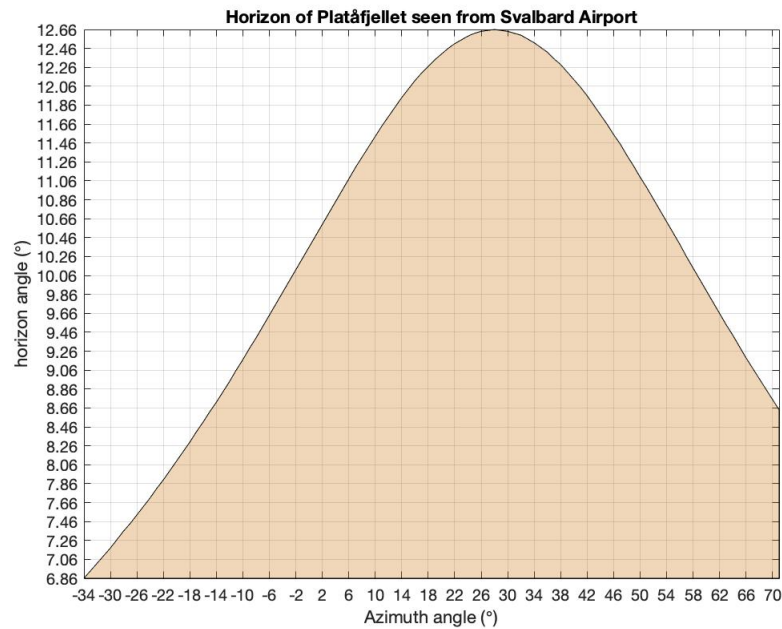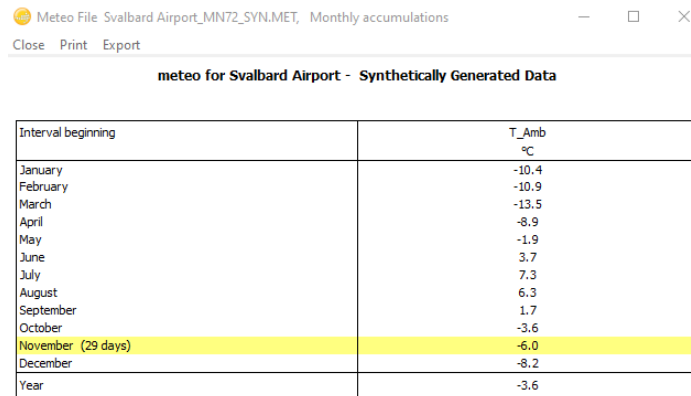
Figure 15: Plot of the southward solar horizon at Svalbard Airport caused by Platåfjellet

4.3 Parameter sensitivity analysis

This section will discuss how sensitive parameters such as temperature, GHI, and albedo impacts the simulation, as well as the oversizing of inverter power.

4.3.1 Temperature

The meteorological data used in the first simulation are monthly values between 1981-1990 stored in PVsyst. From climate research, it is a clear upswing in mean temperature at Spitsbergen. The ambient temperature has increased by +0.22°C per decade from 1912 to 2007 (Hansen and Holmén, 2010). From what we know of PV technology, an increase in cell temperature decreases the cell efficiency and so decreases energy output. One would, therefore, expect the model that bases its simulation on a colder climate will have a higher energy output.

Interval beginning	T_Amb °C
January	-10.4
February	-10.9
March	-13.5
April	-8.9
May	-1.9
June	3.7
July	7.3
August	6.3
September	1.7
October	-3.6
November (29 days)	-6.0
December	-8.2
Year	-3.6

Figure 16: Synthetically generated monthly meteorological data.

Looking at average 2019 temperatures compared to synthetically generated data used in PVsyst, there is a tendency of slightly higher temperatures in 2019. April had the most substantial deviation, with a 5.0°C difference. Other months where solar conditions are good at Longyearbyen, such as May, June and July, the differences are less significant.

Month	Average temperature
January 2019	-10.3°
February 2019	-11.1°
March 2019	-12.6°
April 2019	-3.9°
May 2019	-2.3°
June 2019	4.8°
July 2019	8.4°
August 2019	6.2°
September 2019	2.6°
October 2019	-4.6°
November 2019	-7.2°
December 2019	-10.8°

Figure 17: 2019 average monthly temperatures at Svalbard Airport (Yr, 2020).

.

The simulated average ambient temperature for each month is shown in figure 16, and is based on data from the meteonorm 7.2 database. Average measured temperature Svalbard Airport 2019 is shown in figure 17, published by yr.no (Yr, 2020).

4.3.2 Cell efficiency based on Meteo data and 2019 temperature

The temperature coefficients for the solar modules are -0,35%/°C for the SPR-E20 and -0,41%/°C for the JKM265. With respective efficiencies of 20,4% and 16,19% at STD. Looking at April as an example, the ambient temperature used in PVsyst is at -8.9°C. The difference in the April temperature between the PVsyst average temperature and STD is 28.9°. The change in efficiency for the SPR module is then $0,35\%/°C * 28,9°C = 10\%$. An increase in cell efficiency of 10% makes the total cell efficiency increase from 20,4% to 22,44%. For the JKM module, the increased cell efficiency for April is $0,41\%/°C * 28,9°C = 11,85\%$, which gives an average cell efficiency in April of 18,11%. In table 1, efficiencies for the solar modules are shown for months with solar irradiation.

Table 1: Monthly average module efficiencies.

Month	SPR-E20 efficiency simulation	SPR-E20 efficiency 2019	JKM efficiency simulation	JKM efficiency 2019
March	22,78%	22,72%	18,41%	18,34%
April	22,44%	22,10%	18,11%	17,78%
May	22,05%	22,08%	17,64%	17,67%
June	21,66%	21,58%	17,27%	17,20%
July	21,40%	21,32%	17,03%	16,96%
August	21,47%	21,48%	17,10%	17,11%
September	21,80%	21,74%	17,41%	17,34%
October	22,18%	22,25%	17,76%	17,82%

In April, the average module efficiency was 0,24% higher for the SPR-module and 0,33% higher for the JKM-module in simulation. Based on temperature and cell efficiency, one would expect that the higher temperature in 2019 compared to the generated temperature in PVsyst would lead to the simulation performing better, with April as the primary month for deviation.

4.3.3   GHI at Longyearbyen

To properly assess the difference in electric power production between the power plant and the simulation, it is necessary to look how the GHI values used in the simulation compared to actual GHI at Longyearbyen.
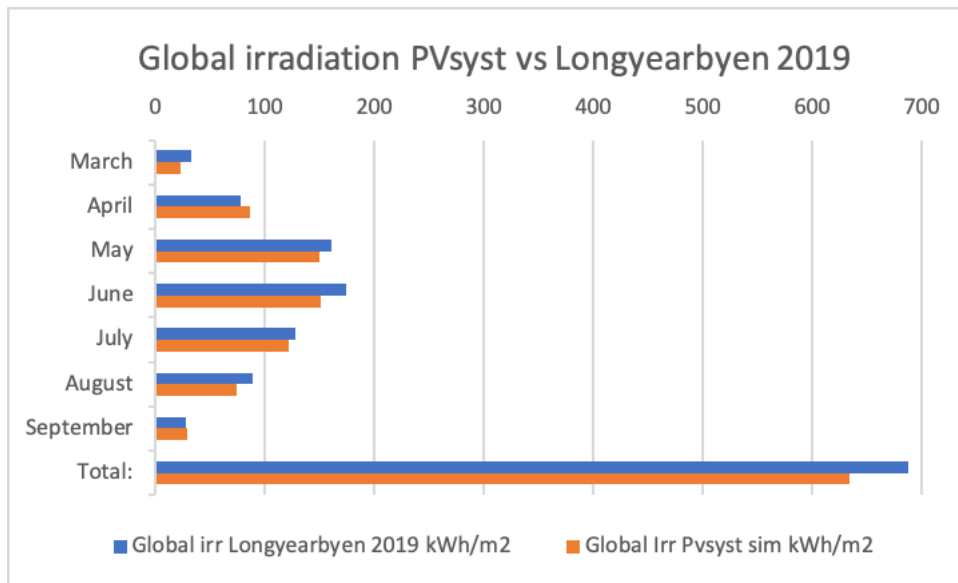
Figure 18: Monthly and total incoming GHI for Longyearbyen 2019 and PVsyst simulation.

At Longyearbyen, the total GHI in 2019 from March to September was 687,45 kWh/m^2, compared to the 633,30 kWh/m^2 synthetically generated GHI in PVsyst (figure 16). The GHI was higher in 2019 for all months except April. Solely based on GHI, one would expect the yield from the power plant to be higher.

Since 2019 was such a good year for solar irradiation compared to the Meteonorm data, an average of the GHI measured by the weather station at Longyearbyen can be made to check if 2019 was a particularly good year in recent times as well. The station started measurements in October 2012. Due to lack of data in early 2012 and as well some time periods in 2018, an average GHI is made from 2013-2017 plus 2019. Later in the assignment, average data from 2015-2017 is implemented in PVsyst to better represent an average year for GHI at Longyearbyen. The reason only three years is loaded into PVsyst is lightly discussed in section 3.3.1. In figure 19, the data is averaged to monthly values, and small holes in the data series do not affect the total average for a particular month. When the data is implemented in PVsyst later, the data needs to be averaged over hourly values. The weather station is publishing 5-minute data points, and the only three years with a

full set of data for every hour was 2015, 2016 and 2017. A solution is to go into the dataset, find the holes and assign them average values of the days before. It is very time-consuming work since the set exists of data points every 5 minutes, and was not prioritised in this thesis.
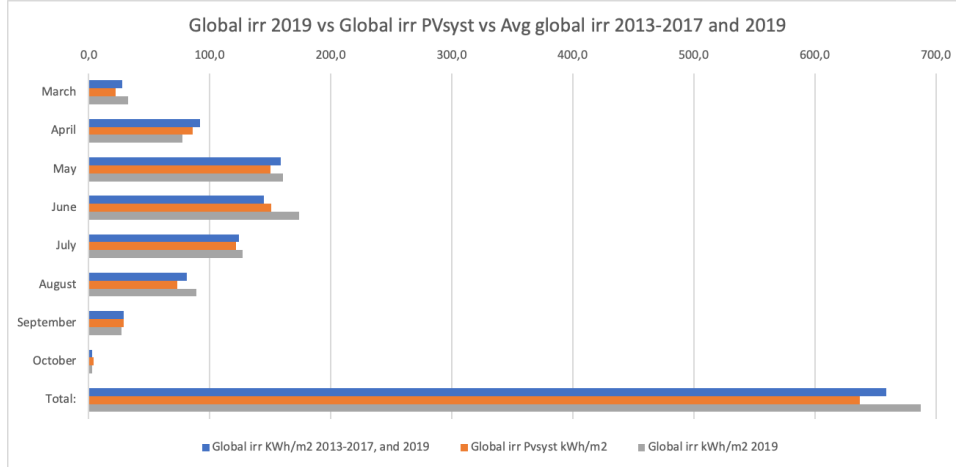
Figure 19: Average GHI compared to GHI in 2019 at Longyearbyen.

From figure 19 it is clear that overall, 2019 was a strong year for solar power. There are two outliers, April as a particularly bad month for solar energy, and June as a solid month. During the weather stations lifetime the measured GHI has been closer to the synthetically generated data by Meteonorm, but still significantly more, 3,4% with 658,9 kWh/m^2 compared to 637,1 kWh/m^2.

4.3.4 Albedo

The overall high albedo at Longyearbyen due to snow cover is one of the main advantages of solar power there. The paper does not use any data for monthly albedo at the plants location, so the albedo will be changed to fit with reality. For the first simulation, the albedo used is shown in figure 20. The albedo value varies from year to year due to seasonal differences in climate. The albedo will be adjusted within realistic levels in later simulations to fit the system with the electric production from 2019.

36
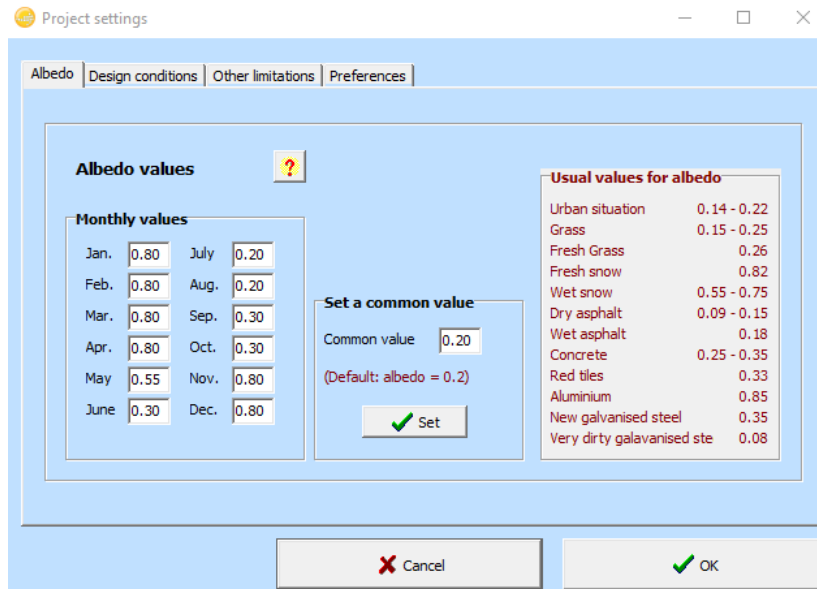
Figure 20: Albedo numbers used in simulation 1.

PVsyst provides guidelines for which albedo values are suitable for different environments. As seen in figure 20, there are a variety of recommended albedo values for different surfaces. For surfaces one can expect to see around the solar plant at Svalbard Airport, fresh snow has the highest albedo. The airports landing strip is located right in front of the solar modules. Dry asphalts albedo value is between 0.09-0.15, so the albedo value for the months of June to September might need to be adjusted to fit with the most prominent conditions around the Airport.

4.3.5 Inverter

In the design of 70 JKM 265Wp solar modules on hangar 1, three 10kW inverters was installed for handling 18.5 kWp. This is a large oversizing of inverter power with respect to the load from the modules. The inverters perform at their maximum efficiency closer to their maximum load (energySage, 2016), and at peak performance from the 70 JKM solar modules, the load on each inverter is only 6 kW. PVsyst does not allow one to run a simulation with highly oversized inverter power, so the inverters are scaled down for the model in PVsyst.

4.3.6 Snow cover

When the project started in 2016, 32 SPR-E20-327 modules with a total power of 10,4 kWp were mounted on the terminal roof with an angle of 15°. These modules are prone to snow cover in during spring and fall. PVsyst does not take into consideration snow cover on modules, so this, along with oversized inverters, will most likely make the simulation more efficient than the actual solar plant.

4.4 First simulation

The first goal of the project was to accurately simulate the solar plant in PVsyst by comparing the results with actual energy yield. In this simulation of the system meteorological data from Meteonorm 7.2 is used, and monthly albedo values chosen for anticipated ground reflection.

4.4.1 Results simulation one

Table 2: Solar energy power production in second simulation compared to power production in 2019 for Svalbard Airport.

System	Terminal/Tower sys	Hangar sys	Total
Svalbard Airport (MWh)	37,88	30,43	68,31
Simulation (MWh)	40,32	34,43	74,75
Difference %	+ 6,44 %	+ 13,1 %	+ 9,42 %

In table 2, one can see that the electric production in simulation is 9,42 % higher than in 2019, which is significant. Several factors are causing this deviation. GHI and temperature deviates from 2019 meteorological data and affects the production of electric power from solar modules. Additionally, the albedo picked in the simulation is a factor of uncertainty. It is difficult to

set correct albedo values for each month as snow colour and time of melting influences the amount of reflection. Further, the oversizing of some inverters used at the Airport will cause a suppressed output. Lastly, moving objects which can cause shade on modules at the Airport is not implemented in the model. These factors are discussed more thoroughly in section 4.3.

4.4.2 GHI and power output
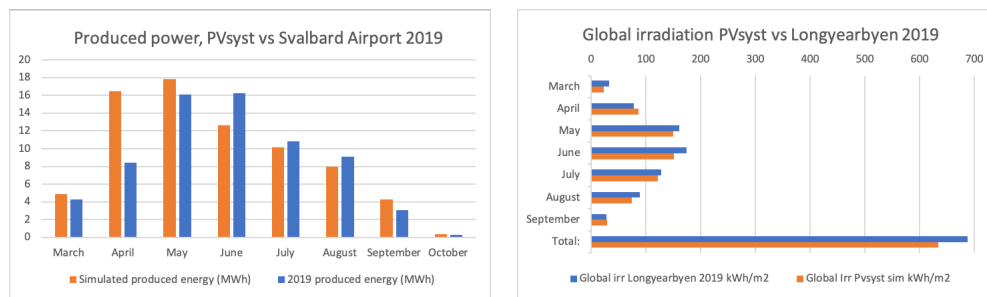
Figure 21: Relation between monthly produced energy and global irradiance for the power plant and simulation.

Figure 21 shows that for April, the electric production at the Airport was over half of what PVsyst simulated for the system. Fittingly, this was also the month where the simulated GHI was high compared to 2019 levels for April (4.3.3), albeit the difference in produced power is a lot larger than the difference in GHI. For May, the GHI was higher in 2019 than the data from PVsyst, but the produced energy was higher for the simulation, suggesting the albedo might be too high. The measured GHI in June 2019 was also higher than for PVsyst, but for this month the production was higher than in the simulation, as one would expect. One reason might be that the albedo for June is more in line with reality. As well, June compared to May is less prone to the possibility of snow cover of modules.

4.4.3 Temperature and cell efficiency

It is worth noticing that vast difference in energy output in April coincides with a significant difference in temperature (4.3.1). With a cell efficiency 0,24% and 0,33% higher in the simulation for April, the temperature dif-

ference between simulation and real temperature amplifies the deviation in power production for April.

4.4.4 PR sim 1
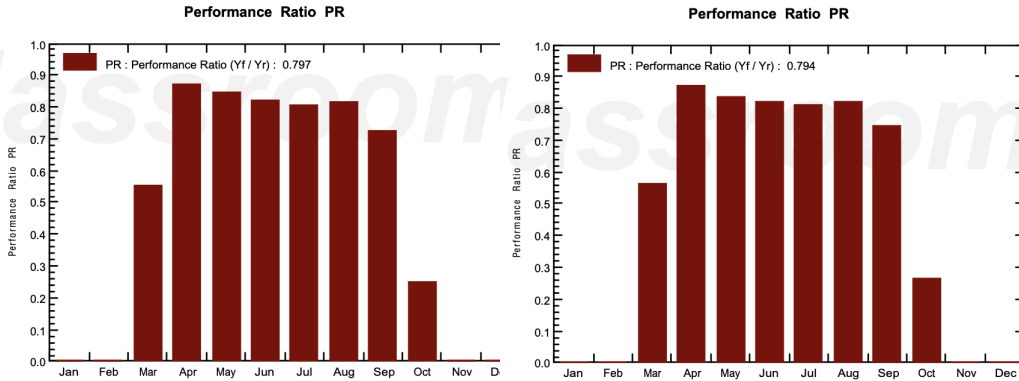
Figure 22: To the left is PR for the hangar system, and to the right is PR for the terminal system in simulation one.

Combined PR for the system is 79,55%.

4.5 Second simulation, using local weather data

Although the results from simulation one were 9,42 % higher than actual yield, there are as discussed plenty of uncertain factors. For this simulation, weather data from Longyearbyen in 2019 are loaded into PVsyst to make the simulation more adjusted to 2019 conditions.

4.5.1 Results simulation two

However, this simulation led to a higher deviation between simulated and real results. The increase in GHI is outweighing the increase in temperature. Interestingly, in figure 23 there is a substantial difference in power in April and May, but for other months results are closer to the real output. Also, using meteorological data from 2019 leads the yield from simulation to be more consistent with actual results, albeit the total difference in yield for the whole year is greater. Looking at table 3, the system consisting of modules on the terminal and tower building has made a jump from 6,44% to 15,15%

Table 3: Solar energy power production in second simulation compared to power production in 2019 for Svalbard Airport.

System	Terminal/Tower sys	Hangar sys	Total
Svalbard Airport (MWh)	37,88	30,43	68,31
Simulation (MWh)	43,62	35,49	79,11
Difference %	+15,15 %	+ 16,6 %	+ 15,8 %
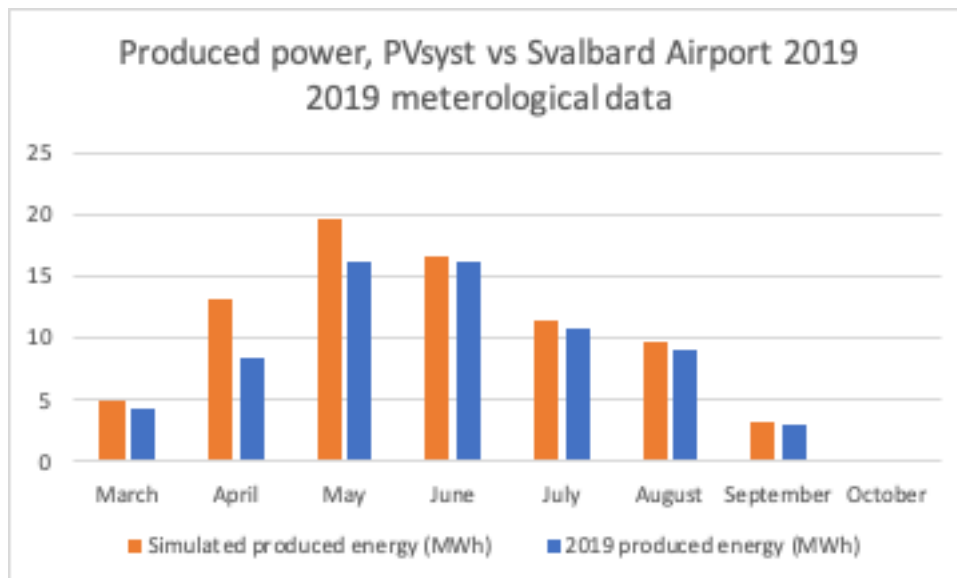
Figure 23: Monthly power production in simulation and Airport 2019 with meteorological data from Longyearbyen.

higher production in simulation. Since most of the difference in power output is in months where the temperature is hovering under and above zero degrees, albedo values implemented in the simulation may be too high.

4.5.2   PR sim 2
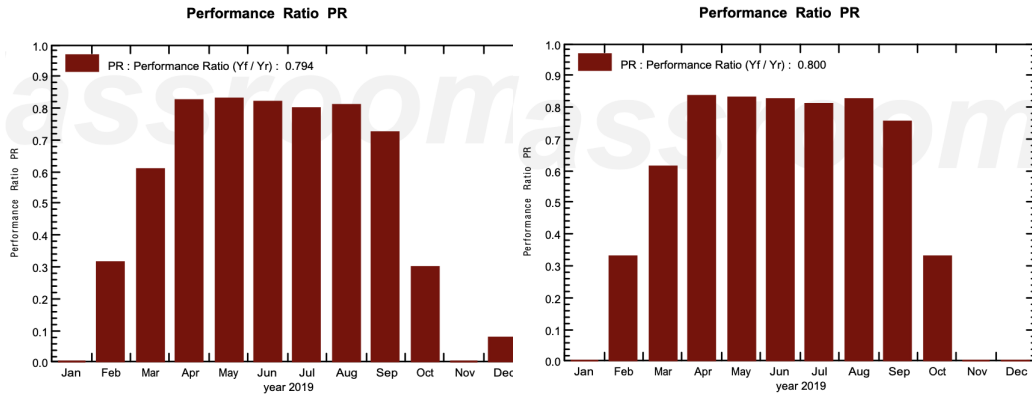
Figure 24: To the left is PR for the hangar system, and to the right is PR for the terminal system in simulation two.

Combined PR of 79,7%. When implementing meteorological data from UNIS, the model is anticipating a production of solar power in February. There is no production in February in simulation 1, but data from the actual plant shows a small yield in February 2019 (Fronius, 2020) As well the report gives a PR in December for the hangar system, although there is no production this month.

4.6   Third simulation, adjusted albedo

In the third simulation, changes in the albedo values are applied to the model. In figure 23, the months with the most substantial deviation are in spring and fall. New albedo values for March, April and May can account for darker areas in and around the Airport. The runway on the Airport is located right in front of all wall-mounted modules facing south-west. The snow layer on the runway melts away when the sun shines directly on the runway, and so decreases the albedo values around these modules instantly. Talking to the airport manager Carl-Einar Ianssen about ground conditions in spring, the runway tends to be snow-free around the first part of April. Generally, snow precipitation occurs on the runway after the initial melting, but this snow/ice melts quickly again due to warm weather and mechanical work on the runway. The new values are found in figure 25.
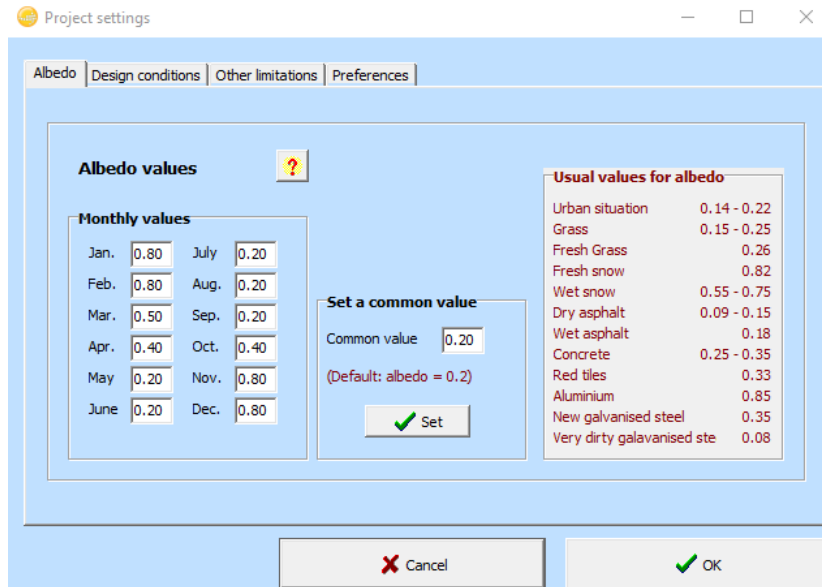
Figure 25: Adjusted albedo values for simulation 3.

4.6.1 Results from simulation three

Table 4: Solar energy power production in third simulation compared to power production in 2019 for Svalbard Airport.

System	Terminal/Tower sys	Hangar sys	Total
Svalbard Airport (MWh)	37,88	30,43	68,31
Simulation (MWh)	41,80	33,06	74,86
Difference %	+10,3 %	+ 8,6 %	+ 9,6 %

The adjusted albedo has led to a decrease in power production in the simulation of 4,56 MWh, resulting in a difference of 9,1%, seen in table 4. There is still a significant gap in March, April, May and October, albeit the deviation is lower than before. The most concerning month is April. There might be both similar and separate issues for the two models that causing the gap.
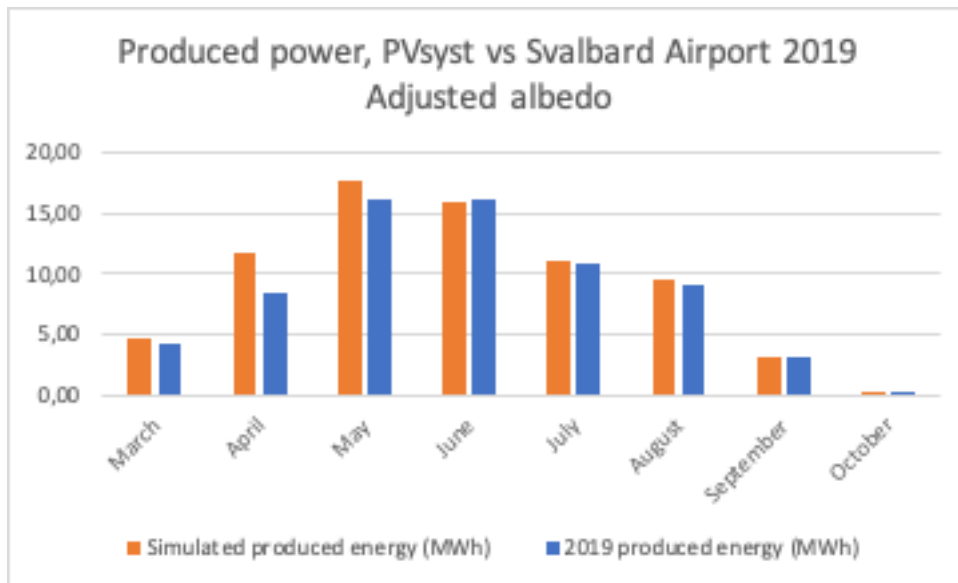
Figure 26: Monthly power production in simulation and airport 2019 with adjusted albedo.

The hangar system has oversized inverters, but this issue should be constant for all months. The tower/terminal has roof-mounted modules that are vulnerable to snow precipitation during winter months. Wall-mounted modules are not as sensitive to this problem.

Table 5: Difference in monthly values between simulation and real life production of energy in simulation three.

| Month	Difference
March	10,5%
April	42,4%
May	10,5%
June	-1,3%
July	3,8%
August	4,4%
September	5,4%
October	14,4%

4.6.2 PR sim 3
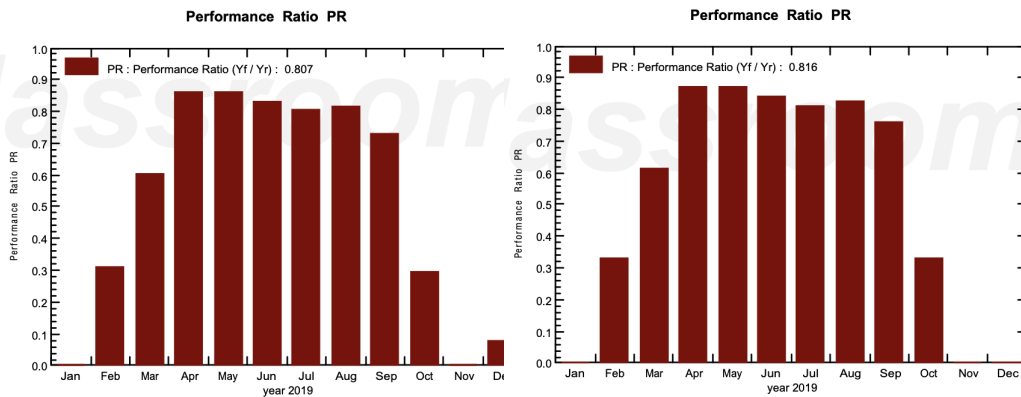
Figure 27: To the left is PR for the hangar system, and to the right is PR for the terminal system in simulation two.

New combined PR 81,15%.

4.7 Fourth simulation, assessing inverter influence

As mentioned in section 4.3.5, three 10 kW inverters were designed to control a 18,5 kWp system. A separate model was made in PVsyst for this system solely, to assess the loss in power production from these modules. In the previous simulation, the power production from the hangar system was simulated 8,6 % above actual production in 2019.

4.7.1 Results for fourth simulation

Table 6: Power production in fourth simulation for modules with oversized inverters.

System	70 JKM-265 mod
Svalbard Airport (MWh)	8,56
Simulation (MWh)	10,10
Difference (%)	18,00%

It is clear from table 6 and figure 28 that the excess inverter power severely halts the power yield from the 70 JKM265 modules. The simulation produced 18% more power than the actual system, which is 9,4% higher than the total difference in production for the hangar system (table 5). Installing correctly sized inverters should at least improve the power yield to somewhere around 8,6% below simulated power output, which is an improvement of 700 kWh. Otherwise, the production follows the same pattern as in simulation three, with significant deviations between simulation and actual results in spring, and a more even power output for the summer.

4.8 Fifth simulation, assessing snow cover

One reason for the massive difference in power yield for spring might be that modules have been covered by snow for some time during this period. For wall-mounted modules, this should not be a significant problem, but for the 32 roof-mounted modules, it might be a more prominent problem. The 32 roof-mounted SPR-E20 modules are controlled by a 20 kW inverter which controls 24 wall mounted modules as well. It is not possible to only extract
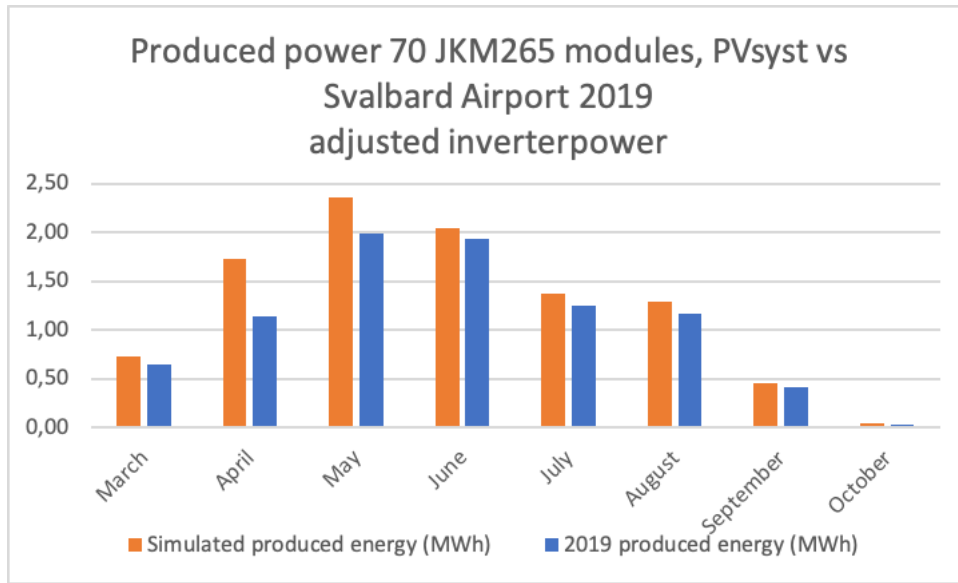
Figure 28: Monthly power production in simulation and airport 2019 adjusted inverter power.

the power yield from 32 roof-mounted modules, but the inverter output from all 56 modules is provided. The same system is made in PVsyst to compare.

4.8.1 Results from fifth simulation

Table 7: Power production in fifth simulation for modules prone to snow cover.

System	32 roof- and 24 wall-mounted mod
Svalbard Airport (MWh)	9,10
Simulation (MWh)	11,04
Difference (%)	21,31%

Overall, the power production in the simulation was 21,31% higher. For March, April and May, the production was respectively 49%, 87% and 25% higher in the simulation. Looking at the differences for monthly production in table 5, the percentage difference is almost five times higher in March, over
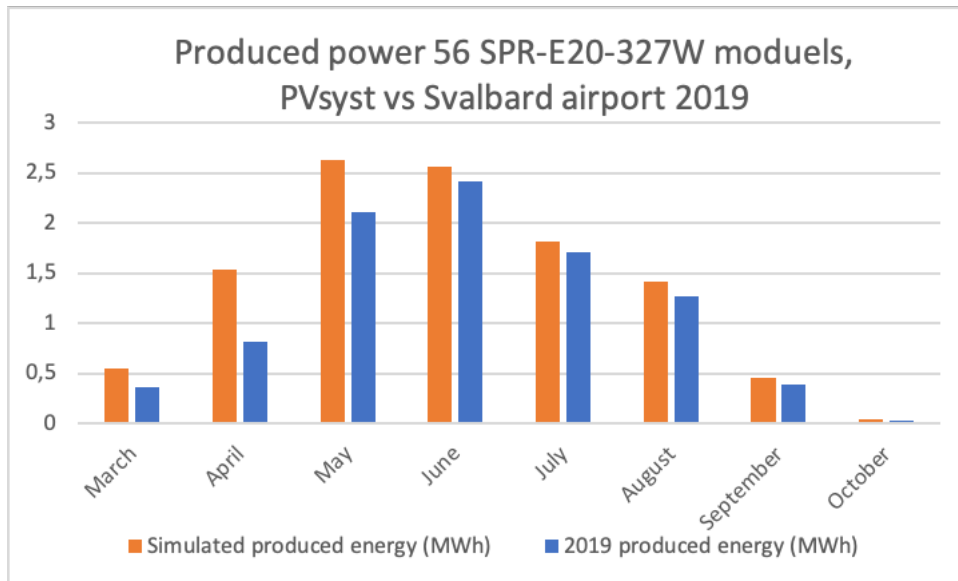
Figure 29: Monthly power production in simulation and airport 2019, 32 roof mounted and 24 wall mounted SPR-E20-327 modules.

twice the size in April and 2,5 times higher in May. September and October delivered well above results in simulation three as well. These months are highly likely to consist of days with snow precipitation, so snow cover is likely to cause a depressed power output. When speaking to the airport manager about the roof-mounted modules, he says they are covered by snow during the winter period, but start producing electricity in March. These are also the modules that were installed when the project first started in 2016 and would be the modules with the most degradation.

4.9 Total impact of oversized inverters and snow cover

For the 70 JKM modules which had the 10 kW inverters, an increase of power to the mean percentage difference with simulated power yield gave an increase of 700 kWh during 2019. For the modules covered by snow, the total power yield was 21% higher in the simulation. If these modules increased their production so that the difference was equal to the total difference for terminal and tower in simulation three (9,5%), the power yield would increase with 945 kWh for the year. Combined inverter loss and snow cover loss stands for a total loss of 1,645 MWh for the Airport. If this loss of power is added

48

to the real power output in 2019, it adds up to 69,96 MWh. The simulated power production in simulation three is then 6,84% higher than the added 2019 power production.

4.10   Summary of model

Although there is still a significant difference in yield between simulation and actual production, the PVsyst model is well balanced with the real system for all months except for April. The PR of 81,15% found in simulation three is reachable for high-quality solar energy plants. Which means that the simulated energy yield is not unrealistic to reach. Actually, in June, Svalbard Airport performed better than in the model. The biggest concern is the deviation in April. It is an anomaly compared to the other months when comparing the simulation with the Airport system. When asking the airport manager about the energy yield in April 2019, he could not recollect if anything was wrong with the plant.

Figure 30: Modules on hangar.

The 6,84 % difference can stem from several factors. The simulation does not account for the degradation on the modules. The project is new, but solar modules typically undergo short-term degradation in their first year, ranging from 1% to 3% (Stahley, 2019). All modules are installed prior to or in 2018. Another cause for the decreased output is shading from moving objects. Modules mounted low on either the hangar or terminal might be exposed for shading from either airplanes or other moving objects in and around the runway. Another cause of uncertainty is the model of the horizon south of the Airport. In table 5, there is a trend for summer months, producing more accurate results in simulation. For months where the sun shines at a lower angle, the difference in results between simulation and real production is more substantial. Which might suggest that there are mountains which cast shade on the Airport for a more extended period than the horizon implemented in the simulation does.

4.11   Study of generic 10kW system, Longyearbyen

Further, the study takes a look at how bifacial modules would fit into a climate such as Longyearbyen. Shading between modules is included for both models, discussed in section 3.5. Albedo found from simulation three is applied to the new models, and the same values are implemented directly under the modules. Meteorological data from the UNIS weather station is used again. An average of the GHI and temperature for the years 2015-2017 is loaded into PVsyst, explained why in 4.3.3. The PR is not included in results for the bifacial modules because PVsyst cannot calculate a correct PR for bifacials. PVsyst only uses front side GII for calculating PR, thus the rear side irradiation on bifacials can increase the PR ratio too over 100%.

Specifications of parameters in simulations:

- Modules are elevated 1 meter above the ground for all simulations with bifacial modules.

- Shading limit angle is 11.6° for all simulations except for tilts 0° where the shadow limit angle is 0°.

- Pitch length for standard modules:

  - 90°: 7,65 m.

– 60°: 7,40 m.

  – 30°: 5.20 m.

  – 0°: 1,55 m.

- Pitch length for tilts on bifacial modules:

  – 90°: 10,00 m.

  – 60°: 9,65 m.

  – 30°: 6,75 m.

  – 0°: 10,00 m.

- Number of sheds = 4 for all simulations.

4.11.1 Results for 10kW standard monofacial module model, SN orientation

Table 8: Results from simulation of the generic 10 kW system with standard modules, SN orientation.

Standard modules, Longyearbyen, SN orientation	Tilt 90°	Tilt 60°	Tilt 30°	Tilt 0°
Yield (kWh/kWp/year)	584	743	758	614
PR (%)	83,35	89,57	93,60	92,68
GCA	0,20	0,21	0,30	1,00
Ground area (m^2)	192,8	187,2	132,4	52,08
Yield per area (kW/m^2/year)	31,64	41,53	59,89	120,5

4.11.2 Results for generic 10kW bifacial model, SN orientation

Table 9: Results from simulation of the generic 10 kW system with bifacial modules, SN orientation.

Bifacial modules, Longyearbyen, SN orientation	Tilt 90°	Tilt 60°	Tilt 30°	Tilt 0°
Yield (kWh/kWp/year)	827	890	831	677
GCA	0,20	0,21	0,30	0,30
Ground area (m^2)	214,2	213,9	157,1	228,6
Yield per area (kW/m^2/year)	43,23	46,61	59,20	33,16

4.11.3 Results for generic 10 kW bifacial model, 45° orientation

Table 10: Results from simulation of the generic 10 kW system with bifacial modules, 45° orientation.

Bifacial modules, Longyearbyen, 45° orientation	Tilt 90°	Tilt 60°	Tilt 30°	Tilt 0°
Yield (kWh/kWp/year)	772	814	760	675
GCA	0,20	0,21	0,30	0,30
Ground area (m^2)	214,2	213,9	157,1	228,6
Yield per area (kW/m^2/year)	40,37	42,64	54,17	33,07

4.11.4   Results for generic 10 kW bifacial model, EW orientation

Table 11: Results from simulation of the generic 10 kW system with bifacial modules, EW orientation.

Bifacial modules, Longyearbyen, EW orientation	Tilt 90°	Tilt 60°	Tilt 30°	Tilt 0°
Yield (kWh/kWp/year)	727	722	656	675
GCA	0,20	0,21	0,30	0,30
Ground area (m^2)	214,2	213,9	157,1	228,6
Yield per area (kW/m^2/year)	38,05	37,82	46,72	33,07

4.11.5   Summary of generic 10 kW systems

For the standard mono facial modules oriented SN, the most optimal tilt of the ones tested was 30°. For the bifacial modules, the SN orientation had the best results for all tilts, with 60° delivering the best yield. The 30° tilt delivered the best yield per m^2 occupied. When the orientation is EW, the optimal tilt changes to 90°, but the yield is significantly less than for other orientations. I believe the 90° degree tilt is the best solution for an EW orientation because the front side of the module only directly faces the sun in the west and east when the sun shines at a low angle, assuming midnight sun. If the module is tilted 90° both sides can harness the maximum amount of the reflected sunlight. It is important to remember that this applies to a system without any horizon and with midnight sun conditions. If somewhere the design of the landscape encourages an EW orientation, a tilt of 90° for bifacial modules might not be the optimal solution, even at a similar latitude to Longyearbyen. Similar to the SN orientation, the 45° orientation's optimal tilt of the ones tested was 60°.

When the tilt is 0°, theoretically there should be no difference in energy yield between orientation because the light is reflected uniformly in all directions from the ground. It is not ideal that the results for orientation SN

and tilt 0° is 2 kWh higher than for 45° and EW orientations. The problem might occur because the calculation on ground point distribution of reflected light is not entirely correct for all pitch sizes in PVsyst.

4.12 Comparison of solar module systems

A comparison is made between the Airport system, the generic standard and bifacial system at Longyearbyen, a similar system in Munich southern Germany and results from mono- and bifacial modules at the UiT.

4.12.1 Results from solar modules UiT

The energy yield per year is plotted by Professor Boström in figure 31. For standard modules at 60°, the yearly yield is approximately 850 kWh/kW. For bifacial modules at 60° the yearly yield is approximately 950 kWh/kW. The modules have been untouched throughout the year, and snow have to slide off the modules naturally. For higher tilt angles the snow slides more easily off the modules, which suits north lying locations where higher tilts are more optimal.
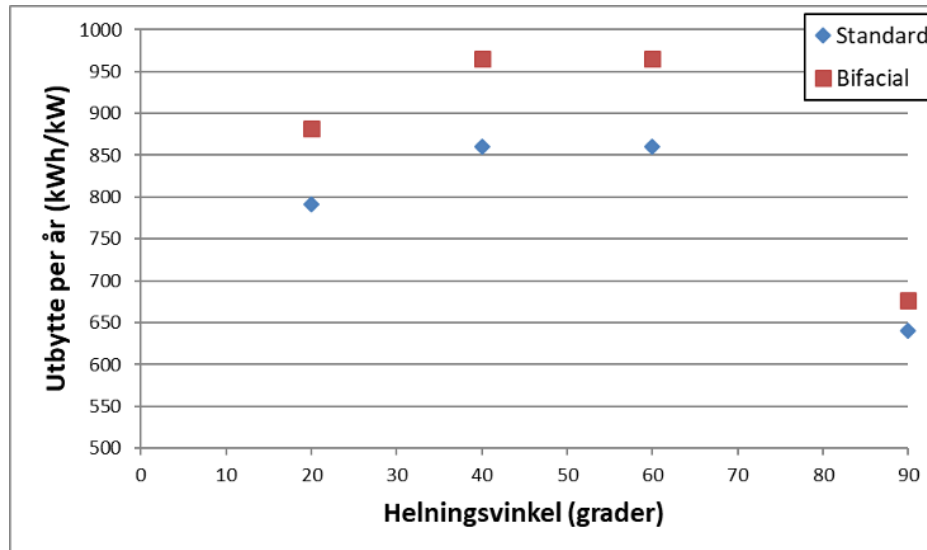
Figure 31: Energy yield in kWh per year per kW installed.

4.12.2 Results from generic 10 kW mono- and bi-facial system in Munich

All albedo values are set to 0.2. All the other parameters are the same as in the 10 kW system at Longyearbyen, which can be found in section 4.11.

Table 12: Results from simulation of the generic 10 kW system with standard modules in Munich, SN orientation.

Standard modules, Munich, SN orientation	Tilt 90°	Tilt 60°	Tilt 30°
Yield (kWh/kWp/year)	776	1102	1205
PR (%)	80,28	85,72	88,84
GCA	0,20	0,21	0,30
Ground area (m^2)	192,8	187,2	132,4
Yield per area (kW/m^2/year)	42,11	61,6	95,23

Table 13: Results from simulation of the generic 10 kW system with bifacial modules in Munich, SN orientation.

Bifacial modules, Munich, SN orientation	Tilt 90°	Tilt 60°	Tilt 30°
Yield (kWh/kWp/year)	1080	1285	1295
GCA	0,20	0,21	0,30
Ground area (m^2)	214,2	213,9	157,1
Yield per area (kW/m^2/year)	56,54	67,27	92,36

4.12.3 Evaluation of yield between locations

Table 14: Yield per kWp installed per year for each location, standard modules.

Standard modules, SN orientation (kWh/kWp)	Tilt 90°	Tilt 60°	Tilt 30°
Simulated Longyearbyen system	584	743	758
UiT real system	640	850	no data
Simulated Munich system	776	1102	1205
Simulated yield from Svalbard Airport	541,5		
Actual yield from Svalbard Airport	498,6		

Table 15: Yield per kWp installed per year for each location, bifacial modules.

Bifacial modules, SN orientation (kWh/kWp)	Tilt 90°	Tilt 60°	Tilt 30°
Simulated Longyearbyen system	827	890	831
UiT real system	675	950	no data
Simulated Munich system	1080	1285	1295
Simulated yield from Svalbard Airport	541,5		
Actual yield from Svalbard Airport	498,6		

For both the standard and bifacial system, the model in Munich provides the best yield. It is worth remembering that the UiT system is up and running, and limitations such as snow cover on modules are included in the results. For mono facial modules, the best tilt in Munich (30°) produced 60% more energy than the best tilt at Longyearbyen (30°), and 41,76% more than the

best modules at UiT campus. The PR in the Longyearbyen system is a little higher than the Munich system. The reason for a higher PR at Longyearbyen is likely due to the low temperature effect and higher albedo values. In the Longyearbyen model, the PR increases as the tilt angle decrease. Although more incident irradiation reaches the module at a higher tilt, the results show that a lower angle is more efficient in a configuration with four sheds. The lower PR may indicate that an increase in tilt decreases the amount of reflected light that reaches the module. The bifacial modules at Longyearbyen had the highest efficiency at 60° tilt, which further backs that the configuration is the cause of the higher yield at 30° tilt. The wall-mounted modules at Svalbard Airport are not affected by shade from other modules, and in that sense not affected by this problem despite the high tilt.

For the bifacial system, the Longyearbyen model with a 90° tilt deliverers almost the same results compared to the UiT system. The wall-mounted bifacial modules at UiT only deliver slightly better results than the mono facial wall-mounted modules at the same site, showing that there needs to be space behind the bifacial modules to utilise the backside of the module. The bifacial modules at 30° tilt in Munich were the best for all tilts tested. The yield was 45,5% higher than the best tilt at Longyearbyen, which for bifacial modules was (60°), and only 36% better than the best modules at UiT campus. These results show that the benefits of installing bifacial systems for locations further north are more profitable than in warmer climates. The increase in yield when switching from standard modules to bifacial is higher in Tromsø and Longyearbyen. The bifacial systems simulated are as well less optimal than the standard system simulated, and potential benefits may be higher than what is found in the simulations. To further increase the efficiency for bifacial systems, the modules can be installed on highly reflective surfaces, like a white TPO (thermoplastic polyolefin) roof, which is an inexpensive thin roofing material, or light coloured stones (Pickerel, 2018). Doing this at Longyearbyen ensures high albedo values for winter and summer. The benefits for a roof-mounted system at Munich is the increased yield per area used. A lower angle on the modules ensure that the modules can be placed tighter together. For limited areas such as a roof, a lower angle is more beneficial. Worth considering is that this is not a linear estimate. If the modules tilted 60° or 90° was simulated tighter together, the yield per area would increase, but the yield in kWh per installed kW and year would decline due to shadow effects.

Comparing the results with the actual and simulated yield at Svalbard Airport shows in some way the difficulty in reaching numbers for an optimal system. The PR found in simulation three of 81% is difficult to surpass, but at the same time, the plant produced a higher yield in June 2019, which implies that the plant had a higher PR in June than the simulation. Most of the modules at Svalbard Airport are wall-mounted, so the most natural thing is to compare it to results from the standard systems with 90° tilt. The actual yield is 35,7% lower at Svalbard Airport than the yield for 90° tilt in Munich. The deviation includes limitations such as abnormally low yield in April, oversized inverters, 360° rotating sun during the summer and snow cover on some modules. The only limitation for the Munich system is the shade from other modules, but this is a lesser problem in Munich than Spitsbergen because the sun's elevation angle is much higher. When instead comparing the simulated Airport system with a 90° standard module system in Munich, the yield is 30,2% lower for the Airport system. I believe this further shows that solar energy is a viable solution to provide green energy in an Arctic climate. Without optimal orientations, and with a horizon casting shade on the system, a complete wall-mounted system produces almost 70% of what an almost optimal 90° degree system in Munich does.

5 Final discussion and conclusion

5.1 Limitations and uncertainties

The results tested against solar energy production at Svalbard Airport show that there is a 9,6% deviation between the model and the solar plant. Furthermore, the study of the model shows there are several factors which decrease the efficiency of the solar energy plant. Oversized inverters and snow cover of modules is proven to cause a decrease in power output during 2019. On the other hand, there are uncertainties which may cause the simulation to perform better or worse. The implementation of the horizon and uncertainties in meteorological data from UNIS account for some of this uncertainty.

5.1.1 Atmospheric effects and quality of GHI data from UNIS

The large AM value at Longyearbyen tells us that less irradiation reach the surface. On the other hand, the air may be cleaner because of low industrial pollution, compensating for the large AM. One thing supporting the case of a cleaner atmosphere are the GHI values gathered from the weather station put up by UNIS. When trying to implement these values into PVsyst, PVsyst would not initially accept the values from the weather station because they were better than PVsyst's clearness index (K_t) for days without clouds. The (K_t) is a measure of clearness in the atmosphere (Böhme, 2019). It is a number between 0 and 1, defined as the surface irradiation divided by the extraterrestrial irradiation (Homer Pro, nd). When the sky is clear, the surface irradiation is higher, leading to a higher clearness index for clear days. Typical K_t values are ranging from 0.25 on cloudy days to 0.75 for clear days (Homer Pro, nd). In figure 32, the blue line represents what clear days K_t values should be at locations with similar AM values such as Longyearbyen. It is easy to spot that many data points are well above the clear day line. At the start, PVsyst would not run any simulations on the MET file created from GHI and temperature data from 2019. I had to manually increase the limits for the allowed number of data points above the clear day line in hidden parameters. Results from the research done by fellow master thesis student Jakob Holden Hansen on solar irradiation in Tromsø, show a lesser amount of the total GHI is reduced in Tromsø compared to more urban locations (Hansen, 2020). Still, some errors might come directly from the pyranometer measuring the GHI. Marius Jonassen at UNIS informed me
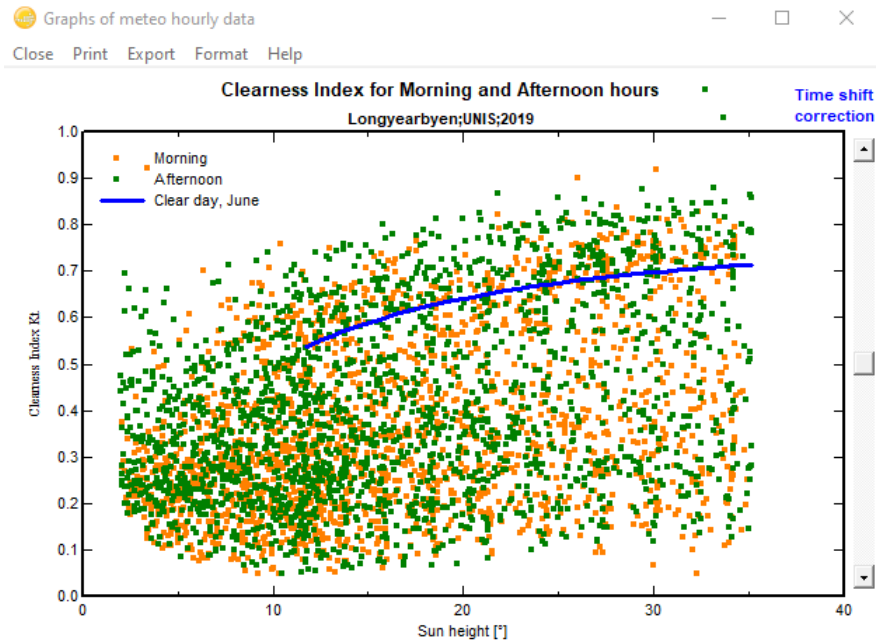
Figure 32: Clearness index for data points from weather station at Longyearbyen

that the pyranometer was last calibrated in fall 2019. The same warning occurs when loading the average GHI from 2015-2017 in PVsyst, so this is not a 2019 issue only.

For many years Longyearbyen existed because of coal mining, but over the years almost all the mines have been closed, with only one left, lying 10 km east from city (Smith-Meyer and Barr, 2020). One-third of the coal from the mine fuels the city with electricity via Longyearbyen energy power plant, which is Norway's only coal power plant (Smith-Meyer and Barr, 2020). Although most of the industrial sector in Longyearbyen is shut down, it is still debatable how much the industrial pollution left at the island influences the atmosphere.

5.2   Summary

A model of the solar power plant at Svalbard Airport has been created in PVsyst and evaluated by running simulations of the model. The process of modelling the airports PV-system began with gathering information about the system, which was provided by the airport manager Carl Einar Ianssen. I was handed data for three construction phases 2016, 2017 and 2018. The horizon was incorporated into the model by using data from "kartverket" on the surroundings of the Airport. After implementing constant data such as solar modules, inverters and orientations, meteorological data measured at Longyearbyen in 2019 were included in the simulation. New albedo values were methodically tested to find the best fit with 2019 conditions. Lastly, specific sub-arrays where concerning factors could restrict the energy output where investigated. The final simulation of the whole system was 9,6% higher than the actual yield. When neglecting factors which limit the production (oversized inverters and snow cover) from the real solar energy system, the simulated plant is 6,84% better.

Based on the model of the Airport, a generic 10 kW system was implemented for Longyearbyen and Munich. The energy yields were compared against solar modules at UiT and the Svalbard Airport system. The results show great opportunities for solar energy in an Arctic climate. The benefits of installing a bifacial system over a standard system is higher in Longyearbyen and Tromsø than Munich. The study also shows that the potential for wall-mounted systems is high in an Arctic environment. Wall-mounted systems are space-efficient and do not suffer from detrimental snow covering. By installing PV's on walls on large buildings facing south with good horizon properties, urban areas can efficiently produce electricity without locking up new space. With an increased willingness to invest in solar energy both in Norway and the world, I hope this thesis can further show that there is an unrealised potential in solar energy in the Arctic. The high electricity price in Longyearbyen is a further incentive to utilise renewable energy there, as well as the global interest in changing the energy sector. With a further decline in solar energy prices and greater awareness in solar energy potential in the north, the amount of solar energy produced at Longyearbyen and the rest of the Arctic sector will hopefully see a further increase in the years to come.

5.3 Further work

There are several possibilities for further work based on the findings in this paper:

- **Further improvements of the system:**
  To further reduce the deviation between real and simulated results, a more in-depth analysis of the actual plant is possible. Based in the model made for the Svalbard Airport system, a thorough investigation of why the energy yield was so low in April 2019 can be looked at.

- **Cost benefit analysis:**
  An economic analysis of the solar energy at the Airport or a new solar project at Longyearbyen can be made. With high electricity prices and decreased costs for PV's, the opportunities for cost-effective solar systems have not been more prominent. How cost-beneficial is the solar energy system at Longyearbyen, and how much can be saved by improving the limitations found in this thesis? Cost-wise, does it make sense to build a solar energy plant with standard or bifacial modules?

- **Analysing the solar energy project against other similar projects**
  This paper has documented the performance of the plant in detail, both for the whole system and for segments. A further study of how the system is performing against other real systems can be made, particularly wall mounted systems.

- **Analysing the clearness index for clear days at Spitsbergen**
  This work is based on the findings when implementing the GHI measurements at Longyearbyen in PVsyst. Why is the measured data for clear days so good? The work can be done by using the same approach as in the thesis done by Jakob Hansen (2020) on the investigation of solar radiation measurements in Tromsø. A pre-study on the pyranometer for potential errors in the measurements can be looked at first to validate the values from the weather station as accurate.

References

Arneth, A., Barbosa, H., Benton, T., Calvin, K., Calvo, E., Connors, S., Cowie, A., Davin, E., Denton, F., van Diemen, R., et al. (2019). Summary for policymakers. *The Intergovernmental Panel on Climate Change (IPCC)*.

Berke, J. (2018). One simple chart show why an energy revolution is coming - and who is likely to come out on top. Accessed: 2020-13-06.

Böhme, L. (2019). Modelling diffuse radiation at high latitudes. Bachelor thesis, Bielefeld University.

electronics, L. (2019). Lg400n2t-j5. `https://www.lg.com/us/business/solar-panels/lg-lg400n2t-j5`. Accessed: 2020-06-04.

energySage (2016). What size solar inverter do i need? `https://news.energysage.com/what-size-solar-inverter-do-i-need/`. Accessed: 2020-04-07.

Fronius (2020). SolarWeb. `https://www.solarweb.com`. Accessed: 2020-10-03.

Hansen, J. H. (2020). Investigation of Solar Radiation Measurements for Sun Tracker System at Nordlysobservatoriet, Tromsø. Master's thesis, University of Tromsø.

Hansen, J. R. and Holmén, K. (2010). Klimaendringer på Svalbard. `https://framsenteret.no/arkiv/klimaendringer-paa-svalbard-4873438-146437/`. Acessed: 2020-13-06.

Homer Pro (n.d.). Clearness index. `https://www.homerenergy.com/products/pro/docs/latest/clearness_index.html`. Accessed: 2020-10-06.

Honsberg, C. B. and Bowden, S. G. (2019). Photovoltaics Education Website.

Jinko Solar (2015). Jkm265p. `https://www.jinkosolar.com/ftp/EN-JKM265P-60(4BB).pdf`. Accessed: 2019-12-05.

Kartverket (2020). Norgeskart. `https://www.norgeskart.no`. Accessed: 2020-03-18.

Laboratory, N. R. E. (n.d.). Solar photovoltaic technology basics. Accessed: 2020-13-06.

LG Solar (2020). Lgenergyfaqs. `https://www.lgenergy.com.au/faq/solar-panels/what-is-an-inverter`. Accessed: 2020-04-06.

Merchant, E. F. (2018). Ipcc: Renewables to suplly 70worst impacts of climate change. `https://www.greentechmedia.com/articles/read/ipcc-renewables-85-electricity-worst-impacts-climate-change`. Accessed: 2020-14-06.

Multiconsult (2018). Solkraft løfter Norge inn i framtiden. `https://www.multiconsult.no/solkraft-lofter-norge-inn-i-framtiden/`. Accessed: 2020-14-06.

Nahar, S. N. (n.d.). Solar Irradiance of the Earth's Atmosphere. *Department of Astronomy, The Ohio State University, Columbus, OH 43210, USA.*

National Snow and Ice Datasenter (2020). Thermodynamics: Albedo. `https://nsidc.org/cryosphere/seaice/processes/albedo.html`. Accessed: 2020-12-06.

Olson, D. (2019). Why the future of solar is bright. `https://www.renewableenergyworld.com/2019/11/12/why-the-future-of-solar-is-bright/#gref`. Accessed: 2020-14-06.

Pickerel, K. (2018). What are bifacial solar modules? `https://www.solarpowerworldonline.com/2018/04/what-are-bifacial-solar-modules/`. Accessed: 2020-06-02.

PVsyst (2019a). Bifacial systems. `https://www.pvsyst.com/help/bifacial_systems.htm`. Accessed: 2020-11-06.

PVsyst (2019b). PVsyst 7 Help. `https://www.pvsyst.com/help/`. Accesssed: 2020-06-03.

PVsyst (2019c). Pvsyst's forum. `https://forum.pvsyst.com/viewtopic.php?t=4235`. Accessed: 2020-11-06.

SMA Solar Technology (n.d). Performance Ratio. Quality factor for the PV plant. *SMA solar Technology AG*.

Smith-Meyer, T. and Barr, S. (2020). Longyearbyen. `https://snl.no/Longyearbyen`. Accessed: 2020-10-06.

Solanki, C. (2015). *Solar Photovoltaics: Fundamentals, Technologies And Applications*. PHI Learning.

Stahley, B. (2019). Commercial solar panel degradation. `https://businessfeed.sunpower.com/articles/what-to-know-about-commercial-solar-panel-degradation`. Accessed: 2020-06-05.

Store Norske Leksikon (2018). Albedo. `https://snl.no/albedo`. Accessed:2020-05-19.

Sunpower (2016). Sunpower E-series. `https://us.sunpower.com/sites/default/files/media-library/data-sheets/ds-e20-series-327-residential-solar-panels.pdf`.

Sunpower (2019). Sunpower Corportation. `https://us.sunpower.com/company/history`. Accessed: 2019-12-05.

Yr (2020). Longyearbyen historic weather data. Accessed: 2020-05-01.

6 Appendices

6.1 A

MatLab code for solar horizon

```
C = 32.4;
a = 0:50.85:5340;
b = 3740;

h_k = sqrt(a.^2+b^2-2.*a.*b*cosd(C));

m_k = 450;

h_a1 = atand(m_k./h_k);
h_a = round(h_a1,2);

azimuth = -34:71;

figure(1)
plot(azimuth,h_a)
axis([-34, 71, min(h_a), max(h_a)])
xticks(-34:4:71)
yticks(min(h_a):0.2:max(h_a))
title('Horizon of Plataajellet seen from Svalbard Airport')
xlabel('Azimuth angle (\circ)')
ylabel('horizon angle (\circ)')
hold on
h = area(azimuth,h_a);
h(1).FaceColor = [0.8 0.48 0.09];
alpha(.3);
grid on
```